Prefusion-specific glycoprotein B human antibodies protect against neonatal HSV-2 infection

Parastoo Amlashi[1,2]†, Jeongryeol Kim[3]†, Nisali N. Mendis[6,7], Perry T. Wasdin[1,2,4,5] Lindsay E. Bass[2], Gwen Jordaan[1,2], Alexandra A. Abu-Shmais[1,2], Matthew D. Slein[3], Nicole V. Johnson[3], Rachel H. Bonami[2,14,15,16], David A. Leib[6], Margaret E. Ackerman[6,7], Jason S. McLellan[3]*, Ivelin S. Georgiev[1,2,4,5,8,9,10,11,12,13]*

[1]Vanderbilt Center for Antibody Therapeutics, Vanderbilt University Medical Center, Nashville, TN 37232, USA

[2]Department of Pathology, Microbiology and Immunology, Vanderbilt University Medical Center, Nashville, TN 37232, USA

[3]Department of Molecular Biosciences, The University of Texas at Austin, Austin, TX 78712, USA

[4]Program in Chemical and Physical Biology, Vanderbilt University Medical Center, Nashville, TN 37232, USA

[5]Center for Computational Microbiology and Immunology, Vanderbilt University Medical Center, Nashville, TN 37232, USA

[6]Department of Microbiology and Immunology, Geisel School of Medicine at Dartmouth, Lebanon, NH 03756, USA

[7]Thayer School of Engineering, Dartmouth College, Hanover, NH 03755, USA

[8]Vanderbilt Institute for Infection, Immunology and Inflammation, Vanderbilt University Medical Center, Nashville, TN 37232, USA

[9]Department of Computer Science, Vanderbilt University, Nashville, TN 37232, USA

[10]Center for Structural Biology, Vanderbilt University, Nashville, TN 37232, USA

[11]Department of Biomedical Informatics, Vanderbilt University Medical Center, Nashville, TN 37232, USA

[12]Department of Chemical and Biomolecular Engineering, Vanderbilt University, Nashville, TN 37232, USA

[13]Department of Biochemistry, Vanderbilt University School of Medicine, Nashville, TN 37237, USA

[14]Division of Rheumatology and Immunology, Department of Medicine, Vanderbilt University Medical Center, Nashville, TN, USA

[15]Vanderbilt Center for Immunobiology, Vanderbilt University Medical Center, Nashville, TN 37232, USA

[16]Vanderbilt Institute for Infection, Immunology and Inflammation, Vanderbilt University Medical Center, Nashville, TN 37232, USA

†These authors contributed equally to this work

*Correspondence: jmclellan@austin.utexas.edu, ivelin.georgiev@vumc.org

ABSTRACT

Herpes simplex virus (HSV) causes severe neonatal infections and long-term neurological issues, with antivirals offering limited efficacy and no approved vaccines. Viral entry requires glycoprotein B (gB) for membrane fusion, yet no human antibodies to the prefusion form of gB have been identified, and antibodies targeting vulnerable epitopes are limited. We used prefusion-stabilized HSV-2 gB and LIBRA-seq technology to analyze B cells from seropositive and healthy donors, discovering four prefusion-specific human antibodies binding unique gB epitopes as determined by cryo-EM. Antibodies 5-18 and 3-6 showed strong cross-neutralization against HSV-1 and HSV-2, offering protection in a neonatal mouse model. These findings highlight the molecular and structural determinants of HSV-2 prefusion gB recognition by human antibodies and demonstrate the translational potential of prefusion-specific gB antibodies.

INTRODUCTION

Herpes simplex viruses (HSV) are enveloped, double-stranded DNA alphaherpesviruses that establish lifelong infection in the peripheral nervous system and cause mucocutaneous disease (*1, 2*). HSV-1 typically presents as orolabial infection, whereas HSV-2 is associated with recurrent genital lesions and episodic viral shedding (*3*). Globally, an estimated 13% of individuals aged 15–49 are infected with HSV-2, highlighting its persistent circulation and high seroprevalence (*4*). Beyond mucocutaneous disease, HSV-2 contributes significantly to morbidity through neurologic complications and severe outcomes in neonates and immunocompromised individuals (*5*). Neonatal HSV-2 infection, most commonly resulting from vertical transmission during birth, can cause long-term neurological impairment or death (*6*). Current treatment relies on nucleoside analogs such as acyclovir, and although high-dose regimens improve survival in neonates, the risks of neurodevelopmental sequelae and relapse remain considerable (*7, 8*). Despite antiviral therapy, disseminated neonatal HSV-2 infection retains a mortality rate of approximately 30% (*7, 9*), underscoring the urgent need for both preventive and adjunctive therapies. In this context, monoclonal antibodies (mAbs) targeting essential viral glycoproteins represent a promising avenue for therapeutic development.

HSV entry depends on a coordinated mechanism involving the surface glycoproteins gB, gD, and the gH/gL complex (*10*). Entry is initiated by the receptor-binding gD, which activates the gH/gL heterodimer to trigger the membrane fusogen gB, a homotrimer that drives fusion of the viral and host cell membranes (*11-13*). gB is highly conserved across herpesviruses and plays a critical role in viral attachment and fusion, making it an attractive target for the development of vaccines and antibodies (*3, 14*). As a class III fusion protein, gB undergoes a large-scale conformational rearrangement from a metastable prefusion state to a stable postfusion state (*15,*

35 *16*). Stabilizing gB in its prefusion state provides a promising strategy for eliciting potent
36 neutralizing antibody responses, as the prefusion conformation presents unique antibody-
37 accessible sites that are concealed or disrupted in the postfusion conformation, as demonstrated
38 for other viral fusion proteins (*17-23*). Indeed, antibodies targeting prefusion-specific epitopes on
39 other viral fusion proteins have been shown to exhibit potent neutralizing activity (*19-23*).
40 However, the structural transition of gB primarily involves domain rearrangements rather than the
41 secondary-structure refolding characteristic of class I fusion proteins, and stabilizing the prefusion
42 state has proven technically challenging, hindering the isolation of prefusion-specific gB
43 antibodies (*24, 25*). Although a camelid nanobody (*26*) and a murine mAb (*25*), both elicited by
44 immunization with recombinant antigens, were recently shown to specifically recognize HSV
45 prefusion gB, it remains unknown whether natural human infection elicits similar prefusion-
46 specific antibody responses and whether such antibodies confer potent neutralization or protection
47 from morbidity and mortality.

48 Although several mAbs protect against HSV-1/2 in preclinical models, most target gD;
49 only a few target gB, fewer still are human-derived, and none are prefusion-specific (*27-32*). The
50 gB ectodomain consists of five structural domains, and most potently neutralizing gB-specific
51 antibodies recognize domains I, II, and IV (**fig. S1**) (*33-35*). Notably, HDIT101, a humanized mAb
52 targeting domain I, did not demonstrate superiority over standard-of-care therapy in a phase 2
53 clinical trial for recurrent genital herpes (*36, 37*). These findings underscore the importance of
54 further delineating the antigenic landscape of prefusion gB and comprehensively profiling the
55 human B-cell response to HSV-2, both of which remain critical for informing next-generation
56 vaccine development and antibody-based interventions.

57 To address these knowledge gaps, we characterized the HSV-2 gB-specific B-cell
58 repertoire in HSV-2 seropositive individuals and healthy individuals with no recorded history of
59 HSV infection. Using the LIBRA-seq (Linking B cell Receptor Sequence to Antigen Specificity
60 through Sequencing) antibody-discovery technology (*38*), we identified four prefusion-specific
61 and two prefusion-preferring antibodies from human peripheral blood mononuclear cell (PBMC)
62 samples. Two prefusion-specific antibodies, 5-18 and 3-6, exhibited potent cross-neutralizing
63 activity against clinical isolates of both HSV-1 and HSV-2. To define the structural basis of their
64 specificity, we determined cryo-electron microscopy (cryo-EM) structures of a prefusion-
65 stabilized HSV-2 gB ectodomain in complex with the antigen-binding fragments (Fabs) of each
66 antibody. Fab 5-18, along with another prefusion-specific Fab 1-14, recognize quaternary epitopes
67 that span domains I and IV of adjacent protomers, whereas Fab 3-6 binds a distinct epitope that
68 bridges domains I and II and the intervening hinge region. Finally, both 5-18 and 3-6 conferred
69 protection in a well-established neonatal mouse model of HSV-2 infection, underscoring their
70 potential as candidate antibody-based interventions to prevent neonatal HSV-2 infection and
71 associated mortality.

72 **RESULTS**

73 **Identification of a diverse set of HSV-2 prefusion gB-specific mAbs by LIBRA-seq**

74 We applied LIBRA-seq to identify HSV-2 prefusion gB-specific B cells from human donor
75 PBMCs. The LIBRA-seq antigen panel included stabilized prefusion and postfusion gB constructs
76 from several clinically relevant human herpesviruses, including HSV-2, human cytomegalovirus
77 (HCMV), and Epstein-Barr virus (EBV), as well as control antigens HIV BG505 gp140 V9.3
78 SOSIP and influenza HA NC99, intended to filter out cells with non-specific binding activity.
79 Prefusion-stabilized gB constructs used were HSV-2 gB-G3 (*39*), HCMV gB C7 (*40*) (PDB ID:

80 7KDP), EBV gB C3-GT (*41*) (PDB ID: 9OAL), as well as the postfusion gB ectodomain base
81 constructs of each herpesvirus. After LIBRA-seq sequencing and computational filtering as
82 previously described (*38*), we isolated a total of 449 antigen-specific B cells from eight donors:
83 three with confirmed HSV-2 seropositivity, three with confirmed HCMV seropositivity, and two
84 healthy donors with no recorded history of HSV or HCMV. A LIBRA-seq score (LSS) of 1 or
85 greater was selected as a cutoff to identify B cells predicted to have specificity for HSV-2 gB. A
86 total of 69 B cells had an LSS ≥1 for HSV-2 prefusion gB, and 75 had an LSS ≥1 for HSV-2
87 postfusion gB, with some B cells having an LSS of ≥1 for both. Of these, we initially selected 22
88 clonally distinct antibodies with diverse sequence characteristics and varying LIBRA-seq scores
89 for HSV-2 prefusion gB and postfusion gB (**Fig. 1A**).

90 These 22 antibodies were produced recombinantly as IgG1 mAbs and screened for binding
91 by indirect enzyme-linked immunosorbent assay (ELISA). The selected antibodies bound either
92 prefusion gB, postfusion gB, or both (**fig. S2A**). To further explore the potential for identifying
93 prefusion-specific human antibodies against HSV-2 gB, we specifically focused on six antibodies
94 that showed: (1) high prefusion and low postfusion gB LIBRA-seq scores (**Fig. 1B**) and/or (2)
95 stronger antibody binding for prefusion than postfusion gB by ELISA (**fig. S2B**). Biolayer
96 interferometry (BLI) experiments were performed to assess the conformational specificity of the
97 isolated antibodies. In these experiments, the IgGs were immobilized to anti-human IgG Fc
98 Capture tips and assessed for binding to prefusion- and postfusion-stabilized HSV-2 gB
99 ectodomains at 200 nM, a concentration sufficient to observe high-affinity interactions. Antibodies
100 5-18, 1-14, 3-6, and 3-5 each displayed saturated binding to prefusion-stabilized gB but negligible
101 binding to postfusion gB, indicative of prefusion-specific binding (**Fig. 1C**). Antibodies 1-13 and
102 5-13 bound both proteins well, but with a faster on-rate for prefusion gB, indicative of a preference

103 for the prefusion conformation. Conversely, anti-HSV gB antibody D48 (*42*) bound both pre- and
104 postfusion gB but had a faster on-rate for postfusion gB. Overall, four antibodies were classified
105 as prefusion-specific and two as prefusion-preferring based on their reactivity to the two stabilized
106 ectodomains, with the BLI data generally in agreement with LIBRA-seq results.

107 To assess how common the HSV-2 gB prefusion-specific and prefusion-preferring
108 antibodies are in the general population, these mAb sequences were compared against a general
109 database of 1.7 million paired antibodies (**fig. S3A**). Several prefusion-specific mAbs exhibited
110 matches with ≥70% HCDR3 identity, most prominently mAb 3-5 (4,498 matches), with fewer
111 matches observed for 5-18 (20 matches) and 3-6 (2 matches), and none for 1-14 (**fig. S3B**).
112 However, no prefusion-specific mAbs shared both heavy and light chain V gene usage with
113 antibodies in the database. Although mAb 5-18 showed multiple VH-matched pairs with high
114 HCDR3 identity, none met the criteria for full clones due to a lack of shared VL usage. Among
115 prefusion-preferring mAbs, 5-13 yielded 163 matches and included a single full clone with
116 matched VH and VL genes and ≥70% CDR3 identity, whereas mAb 1-14 showed no such matches
117 (**fig. S3B**). Together, these analyses suggest that no true public clonotypes could be identified for
118 the prefusion-specific gB mAbs from our study.

119 **Prefusion-specific gB antibodies potently neutralize HSV**

120 To investigate epitope groups on prefusion HSV-2 gB, we performed a pairwise
121 competition ELISA with all 22 antibodies initially identified from the dataset (**Fig. 2A**). The
122 patterns of binding-inhibition among antibody pairs compared to signal with no antibody
123 competition suggested the existence of at least one shared epitope on prefusion gB, as well as
124 clusters of antibodies that target overlapping or closely positioned binding regions (**Fig. 2B**). To
125 further characterize these interactions, we measured the binding affinities of the Fabs to prefusion-

126 stabilized HSV-2 gB via BLI (**Fig. 2C and fig. S4**). Both prefusion-specific and prefusion-
127 preferring mAbs exhibited picomolar affinities for prefusion-stabilized HSV-2 gB. Among them,
128 Fab 1-14 showed the strongest binding, with an equilibrium dissociation constant (K_d) of 0.03 nM
129 and a dissociation rate constant (k_{off}) at the instrument's limit of detection (1.2×10^{-5} s^{-1}).
130 Prefusion-specific Fab 3-6 exhibited a K_d of 0.12 nM and a k_{off} of 5.3×10^{-5} s^{-1}. Given the high
131 sequence similarity between HSV-2 and HSV-1 gB, we produced a prefusion-stabilized HSV-1
132 gB ectodomain construct by applying the same stabilizing substitutions developed for HSV-2 gB
133 (**fig. S5 and fig. S6A-C**). Binding affinities of the antibodies for the prefusion-stabilized HSV-1
134 gB were then determined via BLI by immobilizing HSV-1 prefusion gB to Ni^{2+}-NTA tips and
135 dipping into Fab (**Fig. 2C and fig. S6D**). Fab 3-6 exhibited a slightly improved affinity (K_d = 0.08
136 nM), driven by a faster association rate constant (k_{on} = 9.8×10^5 $M^{-1}s^{-1}$). In contrast, Fab 5-18
137 showed substantially reduced binding to HSV-1 gB, with a faster dissociation rate constant and
138 lower overall affinity (K_d = 40 nM). Fabs 1-14 and 3-5 bound HSV-1 gB with affinities comparable
139 to those observed for HSV-2 gB.

140 We next assessed the neutralization activity of the mAbs against the prototypic HSV-2
141 strain G via plaque-reduction assay (**Fig. 2D**). mAb 3-6 exhibited the most potent neutralization
142 (IC_{50} = 0.29 nM), exceeding well-characterized antibodies such as D48 (IC_{50} = 0.50 nM) and
143 HSV8 (an anti-gD antibody; IC_{50} = 0.51 nM). mAb 5-18 (IC_{50} = 1.25 nM) and 1-14 (IC_{50} = 1.44
144 nM) were also potent and showed comparable neutralizing activity (**Fig. 2E**). In contrast, 3-5 was
145 relatively weakly neutralizing despite having an affinity similar to the other prefusion-specific
146 antibodies. We also evaluated the neutralization activity of these prefusion-specific antibodies
147 against the clinical HSV-1 strain NS. Consistent with results for HSV-2, mAb 3-6 exhibited the
148 most potent neutralizing activity (IC_{50} = 0.34 nM), exceeding that of D48 (IC_{50} = 1.66 nM). mAb

149 5-18 (IC_{50} = 3.30 nM) was the next most potent, followed by 1-14 (IC_{50} = 33.46 nM). In contrast,
150 3-5 did not neutralize HSV-1 NS infection at the concentrations tested. These findings demonstrate
151 that HSV-2 prefusion-specific gB antibodies can cross-react with HSV-1 gB, and that 3-6 is the
152 most potent antibody against both HSV-1 and HSV-2.

153 We next evaluated *in vitro* autoreactivity of the four prefusion-specific gB antibodies to
154 self-antigens using immortalized human epithelial cell lines. We determined intracellular and
155 extracellular IgG binding to live, permeabilized HEp-2 and HEK293T cells by flow cytometry. At
156 25 µg/mL, none of the prefusion-specific gB antibodies displayed extracellular binding to either
157 cell line (**Table S1**). Although mAbs 1-14 and 5-18 exhibited low levels of intracellular binding
158 compared to the positive control antibodies 4E10 and 2F5, no such reactivity was observed for
159 mAbs 3-5 and 3-6 (**fig. S7**).

160 **Antibodies 5-18 and 1-14 recognize quaternary epitopes spanning domains I and IV of**
161 **adjacent protomers**

162 We determined cryo-EM structures of prefusion-stabilized HSV-2 gB ectodomain in
163 complex with Fabs 5-18 and 1-14 at 2.9 Å and 3.2 Å resolution, respectively, to investigate the
164 molecular basis of their prefusion-specific epitopes (**Fig. 3**, **fig. S8 and fig. S9**). Both antibodies
165 recognize quaternary epitopes spanning domains I and IV of adjacent protomers, but through
166 distinct interaction modes. Fab 5-18 makes extensive contacts with both domains, burying a total
167 surface area of 1,440 $Å^2$, with 835 $Å^2$ on domain I and 605 $Å^2$ on domain IV (**Fig. 3A-B and fig.**
168 **S10A**). The antibody forms 14 hydrogen bonds and 4 salt bridges with domain I and 10 hydrogen
169 bonds with domain IV (**Table S2**). All three complementarity-determining regions of the heavy
170 chain (HCDRs) engage domain I. HCDR1 and HCDR2 recognize domain I, whereas HCDR3
171 spans domains I and IV (**fig. S10B**). Complementarity-determining regions of the light chain

172 (LCDRs) 1 and 3 primarily interact with domain I, whereas LCDR2 interacts extensively with
173 domain IV, establishing a continuous hydrogen-bond network that stabilizes the interface (**fig.**
174 **S10C).** This distribution of the epitope on to adjacent protomers suggests that binding of 5-18, as
175 well as 1-14, prevents protomer separation and locks gB in the prefusion conformation, providing
176 a mechanistic basis for neutralization. Mapping the epitope of 5-18 on to the structure of postfusion
177 gB (PDB ID: 8RH2) reveals that the epitope is disrupted in the postfusion conformation due to the
178 reorientation of domain I relative to domain IV, resulting in contact residues on gB separated by
179 approximately 100 Å (**Fig. 3C**). Additionally, some of the epitope residues on domain I are buried
180 by domain V of an adjacent protomer in the postfusion conformation, collectively providing a
181 structural basis for the prefusion specificity of 5-18.

182 Fab 1-14 has a smaller binding footprint than 5-18, burying a total surface area of 1,125
183 $Å^2$ (**Fig. 3D-E** and **fig. S10D**). Notably, interactions with domain IV differ substantially: 1-14
184 buries 244 $Å^2$ on domain IV versus 605 $Å^2$ for 5-18. The majority of the 1-14 contacts are mediated
185 by HCDR2 and HCDR3, which make extensive interactions with the long loop between β14 and
186 β15 in domain I (**fig. S10E**). LCDR1 and LCDR3 primarily contact domain I, whereas LCDR2
187 and framework 3 (FR3) make limited contacts with domain IV (buried surface area of 121 $Å^2$),
188 including residues in the N-terminal α1 helix (**fig. S10F**). Similar to 5-18, the epitope of 1-14
189 becomes discontinuous and partially buried in the postfusion conformation, providing the
190 structural basis for its prefusion-specificity (**Fig. 3F**).

191 Interestingly, the epitopes of 5-18 and 1-14 closely resemble the epitope targeted by a
192 recently described prefusion-specific gB-directed camelid nanobody Nb1_gbHSV (*26*), which
193 recognizes a quaternary epitope spanning domains I, III, and IV (**fig. S11**). An epitope comparison
194 shows that the Nb1_gbHSV contacts many of the same residues as Fabs 5-18 and 1-14, but the

195 nanobody reaches more deeply into the space between domains I and IV, contacting domain III
196 (**fig. S11E-F**). By contrast, Fabs 5-18 and 1-14 form more extensive contacts across domains I and
197 IV (**fig. S11A-D**). These structural studies reveal multiple solutions by the human and camelid
198 immune systems to recognize a similar quaternary epitope on prefusion gB proteins.

199 **Antibodies 3-6 and 3-5 bind distinct epitopes located within a single protomer**

200 Next, we determined a cryo-EM structure of a ternary complex of prefusion-stabilized
201 HSV-2 gB bound to Fabs 3-6 and 3-5 at a resolution of 3.1 Å (**Fig. 4A and fig. S12**). Fab 3-6
202 engages an extensive interdomain epitope encompassing domains I, II, and the hinge region
203 connecting them, burying a total surface area of 886 Å² (**Fig. 4B and fig. S13A**). Binding is
204 mediated primarily by the heavy chain (806 Å²), with a much smaller contribution from the light
205 chain (80 Å²), involving a total of 16 hydrogen bonds and 1 salt bridge (**Table S3**). The FR1 and
206 HCDR1 of the heavy chain interact with the α4 helix of domain II. HCDR1, HCDR2, and HCDR3
207 form multiple hydrogen bonds with the backbone of hinge residues 351–358, establishing an
208 extensive interaction network (**fig. S13B**). Additionally, $Trp100_{HCDR3}$ is inserted into a
209 hydrophobic pocket in domain I formed by Tyr152, Tyr279, Phe295, and Val352, burying 134 Å²
210 of surface area (**Fig 4B and fig. S13C**).

211 Superposition of domain I from a Fab 3-6-bound protomer onto domain I of the postfusion
212 gB structure shows that domain II reorients in the postfusion conformation and would clash with
213 Fab 3-6 (**Fig. 4C**). The flexible hinge residues at the center of the epitope also undergo a
214 conformation change, distorting the epitope. Collectively, these rearrangements provide a
215 structural basis for the inability of 3-6 to bind trimeric postfusion gB. A recently reported prefusion
216 gB-specific murine mAb named WS.HSV-1.24 (*25*) was shown to recognize a highly similar
217 epitope, but it is rotated about the heavy chain such that the light chain is on the opposite side

218 relative to that of 3-6 (**fig. S14**). Overall, 3-6 targets a highly neutralization-sensitive prefusion-
219 specific epitope encompassing the hinge region between domains I and II, establishing this site as
220 a vulnerable region on HSV-2 gB.

221 Antibody 3-5 binds to an epitope at the tip of domain I, a region not previously known to
222 be targeted by gB-directed antibodies (**Fig. 4A**). This interaction enabled modeling of the domain
223 I residues near the fusion loops, which were disordered in the HSV-2 gB structures complexed
224 with 5-18 or 1-14. Fab 3-5 forms a large interface on domain I, burying a total of 1,296 $Å^2$ of
225 surface area. The heavy chain buries 980 $Å^2$, whereas the light chain buries only 316 $Å^2$. All heavy
226 chain CDRs, as well as FR1 and FR3, participate in the interaction with domain I, forming 16
227 hydrogen bonds (**Table S3**). Residues in LCDR1 and LCDR3 form 7 hydrogen bonds with
228 residues in domain I, further extending the interaction surface (**Table S3**). Interestingly, the angle
229 of approach of Fab 3-5 is oriented upward from the membrane-proximal side, likely preventing
230 binding to the native, membrane-embedded prefusion gB trimer on virions. Furthermore, the
231 epitope overlaps with the membrane proximal region (MPR) helices that sequester the fusion loop
232 residues at the tip of domain I in the full-length prefusion conformation (**Fig. 4D**). This limited
233 epitope accessibility on the native virion could explain the poor neutralizing activity of Fab 3-5
234 despite its high binding affinity for the prefusion-stabilized gB ectodomain construct. The
235 prefusion specificity of Fab 3-5 is explained by the steric clashes between its heavy chain and
236 domain I of the adjacent protomer in the postfusion conformation (**Fig. 4E**). Given that 3-5 is
237 unable to bind postfusion gB trimers and is unlikely to bind prefusion membrane-anchored trimers,
238 this antibody may have been elicited against an intermediate conformation of gB.

239 **Conservation and glycan shielding of HSV-2 prefusion-specific epitopes across human**
240 **herpesvirus gBs**

241 We analyzed the sequence similarity and glycan shielding of the prefusion-specific
242 epitopes on HSV-2 gB targeted by mAbs 5-18 and 3-6 and compared these features across human
243 herpesvirus gBs, focusing on the betaherpesvirus HCMV and the gammaherpesvirus EBV (**Fig.**
244 **S15**). Sequence conservation analysis revealed that the quaternary epitope recognized by 5-18 is
245 highly divergent among these viruses, with only 6 out of 44 contact residues conserved in HCMV
246 and 7 out of 44 in EBV (**fig. S15A**). The epitope targeted by 3-6 also shows low conservation
247 across these viruses, with 4 out of 24 residues conserved in HCMV and 8 out of 24 in EBV.
248 Notably, the hinge region within this epitope is highly variable among human herpesvirus gBs,
249 reflecting the divergent evolution of this site (**fig. S15B**). It is therefore unlikely that broadly
250 reactive, pan-herpesvirus antibodies will be elicited against either site on gB.

251 In addition to sequence conservation, we also analyzed the glycan shielding of these
252 epitopes. HSV-2 gB contains six N-linked glycosylation sites per protomer, four of which are
253 resolved in our structures. Domains I and IV, which are major targets of neutralizing antibodies,
254 lack glycosylation, and the quaternary epitopes recognized by 5-18 and 1-14 remain unshielded in
255 HSV-2 gB (**fig. S15C**). An N-linked glycan at Asn671 is positioned near Fab 3-6, but this does
256 not prevent the antibody from binding (**fig. S15C**). We next examined glycan shielding of
257 prefusion epitopes on HCMV (*43*) and EBV (*44*) gB, for which glycans were modeled using
258 Glycoshape (*45*) (**fig. S15C**). Structural analysis of the 5-18 contact sites on HCMV and EBV gB
259 shows that, although the glycans at Asn586 and Asn555 in HCMV and Asn563 in EBV are
260 positioned at the edge of the contact interface in domain IV, the major contact surfaces of the 5-
261 18 epitope remain largely unshielded in both viruses (**fig. S15C**). In contrast, the 3-6 binding site,
262 particularly the hinge region, contains a glycan in both HCMV (Asn341) and EBV (Asn290),
263 suggesting glycan-mediated masking of a site that is highly vulnerable on HSV-2 gB (**fig. S15C**).

264 Notably, this hinge-region glycan is conserved in HCMV, EBV, and HHV-6, but is absent from
265 HSV-1, VZV, KSHV, and HHV-7, indicating divergent glycan-shielding strategies among human
266 herpesviruses (**fig. S15B**).

267 **Prefusion-specific gB antibodies protect from HSV-2 challenge in a neonatal mouse model**

268 Given the strong neutralizing activity of 3-6, 5-18, and 1-14, we assessed their ability to
269 protect mice from a lethal challenge of HSV2-CNS11, a highly virulent clinical isolate. Briefly, 2-
270 day-old C57BL/6J pups were administered 80 μg of mAb intraperitoneally (i.p), followed by an
271 immediate intranasal (i.n.) challenge with 500 plaque-forming units (PFU) of HSV2-CNS11 (**Fig.**
272 **5**). Each of the three tested prefusion gB-specific mAbs provided statistically significant ($p \leq 0.002$)
273 partial protection at this treatment dose, as compared to the VRC01 control. All animals treated
274 with the negative control HIV-1 envelope-directed mAb VRC01 failed to survive infection. At day
275 21 post-infection, the protection afforded by 3-6 was equivalent to that provided by HSV8 (gD-
276 specific), with an overall survival rate of 91%. Treatment with 5-18 afforded 75% protection,
277 which was comparable to but lower than the 87% protection provided by the gB-specific control
278 mAb D48. Antibody 1-14 provided the least protection (20%). Collectively, these data demonstrate
279 that mAb 3-6 can confer a high degree of protection against a lethal HSV2-CNS11 challenge in a
280 neonatal mouse model, equivalent to that afforded by the gD-directed mAb HSV8.

281 **DISCUSSION**

282 HSV is a widespread and clinically significant human pathogen that disproportionately
283 affects vulnerable populations. Notably, HSV is an etiologic agent of neurologic and neonatal
284 disease, often resulting in lifelong complications and substantial direct and indirect healthcare
285 costs (*46, 47*). Preclinical studies have demonstrated that protective mAbs are highly effective for
286 controlling perinatal HSV infection (*27, 29, 36, 37*); however, the structural and molecular basis

287 of antibody recognition of the viral fusion glycoprotein B (gB)—particularly in its prefusion
288 conformation—remains poorly defined. Here, we describe the identification of human antibodies
289 that recognize epitopes exclusive to prefusion gB and potently cross-neutralize both HSV-1 and
290 HSV-2. Two such antibodies, 5-18 and 3-6, conferred strong protection against lethal HSV-2
291 infection in a neonatal mouse model, further underscoring their therapeutic potential.

292 Prior to this work, prefusion-specific human antibodies targeting gB had not been
293 characterized. This likely reflects both the substantial similarity between the exposed surfaces on
294 prefusion and postfusion gB and the lack of prefusion-stabilized gB probes for B-cell sorting.
295 Recently, a prefusion-specific camelid nanobody and a prefusion-specific murine antibody were
296 isolated following immunization with vesicle-displayed native HSV-1 gB (*26*) or prefusion-
297 stabilized HSV-1 gB (*25*), respectively; however, large-scale screening of human B cells
298 specifically targeting prefusion gB has not been reported. Here, we address this limitation by
299 applying LIBRA-seq with a prefusion-stabilized HSV-2 gB antigen (*39*) to PBMCs from HSV-
300 seropositive donors, enabling the isolation of human prefusion-specific antibodies and the
301 identification of previously uncharacterized vulnerable epitopes on HSV gB. With the recent
302 development of soluble, prefusion-stabilized herpesvirus gB antigens and high-resolution
303 structural information (*39-41*), there is now considerable potential to discover and develop
304 additional potent prefusion gB-specific antibodies. Although prefusion-specific antibodies
305 targeting HCMV and EBV gB may differ from those recognizing HSV-1 and HSV-2 gB due to
306 distinct glycan shielding patterns (**fig. S15C**), it will be important to determine whether similarly
307 potent neutralizing antibodies and discrete prefusion-specific epitopes exist across herpesvirus gB
308 orthologs.

309 Antibodies 5-18 and 3-6 potently neutralized both HSV-1 and HSV-2, with 3-6
310 demonstrating the greatest potency against both clinical isolates (**Fig. 2D-E**). When co-
311 administered with a lethal dose of HSV2-CNS11 in a neonatal mouse study, mAb 3-6 conferred
312 protection comparable to previously characterized neutralizing antibodies HSV8 (gD-specific) and
313 D48 (gB-specific), highlighting its therapeutic potential (**Fig. 5**). Given the multistep nature of
314 herpesvirus entry (*48*), therapeutic strategies employing antibody cocktails that target multiple
315 epitopes within a single glycoprotein or span distinct viral glycoproteins may provide enhanced
316 protection. Because gD mediates viral attachment (*49*) and gD-directed antibodies have been
317 extensively studied and have shown robust neutralizing activity (*28*), combining gD-specific
318 antibodies with prefusion gB-specific antibodies may represent an improved strategy for HSV
319 prevention or treatment. Such combinations would target sequential steps in viral entry and may
320 yield synergistic antiviral effects.

321 In these studies, we determined that the prefusion-specific antibody 3-5 binds a membrane-
322 proximal epitope on gB. Structural analysis indicates that 3-5 is unlikely to engage prefusion gB
323 in the viral membrane, as its predicted angle of approach would result in steric clashes with the
324 lipid bilayer and MPR helices. Consistent with this interpretation, 3-5 exhibits poor neutralizing
325 activity against HSV-2, suggesting that it may recognize an intermediate conformational state of
326 gB, such as after domain I has disengaged from the MPR but before insertion of the hydrophobic
327 fusion loops into the target cell membrane. Intermediate conformations of class III fusion proteins
328 have been visualized by cryo-electron tomography, including for vesicular stomatitis virus G (*50*).
329 Analogously, non-neutralizing prefusion-specific antibodies have been described for HIV-1,
330 where antibodies targeting membrane-proximal gp41 base epitopes are preferentially elicited,
331 thereby constraining the induction of broadly neutralizing responses (*51, 52*). Recent studies

332 further indicate that prefusion-stabilized HSV-2 gB elicits immune responses comparable to those
333 induced by postfusion gB (*39*), underscoring the challenge of selectively focusing humoral
334 immunity on functionally vulnerable prefusion epitopes. Systematic characterization of B cell
335 lineages, coupled with antigen-design strategies such as glycan shielding or epitope masking, can
336 be utilized to preferentially enhance the activation of B cells encoding potently neutralizing and
337 protective antibodies against HSV. Furthermore, the results from these studies suggest that
338 potently neutralizing mAbs targeting the prefusion form of gB represent an attractive therapeutic
339 option for preventing HSV-associated disease in vulnerable populations.

REFERENCES

1. P. G. Arduino, S. R. Porter, Herpes Simplex Virus Type 1 infection: overview on relevant clinico-pathological features*. *Journal of Oral Pathology & Medicine* **37**, 107–121 (2008).
2. D. U. De Rose *et al.*, Neonatal herpes simplex virus infection: From the maternal infection to the child outcome. *Journal of Medical Virology* **95**, (2023).
3. S. A. Connolly, J. O. Jackson, T. S. Jardetzky, R. Longnecker, Fusing structure and function: a structural view of the herpesvirus entry machinery. *Nature Reviews Microbiology* **9**, 369–381 (2011).
4. C. James *et al.*, Herpes simplex virus: global infection prevalence and incidence estimates, 2016. *Bulletin of the World Health Organization* **98**, 315–329 (2020).
5. M.-L. Engman *et al.*, Neuropsychologic Outcomes in Children With Neonatal Herpes Encephalitis. *Pediatric Neurology* **38**, 398–405 (2008).
6. Z. A. Brown *et al.*, Effect of Serologic Status and Cesarean Delivery on Transmission Rates of Herpes Simplex Virus From Mother to Infant. *JAMA* **289**, 203 (2003).
7. D. W. Kimberlin *et al.*, Oral Acyclovir Suppression and Neurodevelopment after Neonatal Herpes. *New England Journal of Medicine* **365**, 1284–1292 (2011).
8. D. W. Kimberlin *et al.*, The Safety and Efficacy of High-Dose (HD) Acyclovir (ACV) in Neonatal Herpes Simplex Virus (HSV) Infections. *Pediatric Research* **45**, 165A–165A (1999).
9. R. Whitley, E. A. Davis, N. Suppapanya, Incidence of Neonatal Herpes Simplex Virus Infections in a Managed-Care Population. *Sexually Transmitted Diseases* **34**, 704–708 (2007).
10. E. E. Heldwein, C. Krummenacher, Entry of herpesviruses into mammalian cells. *Cellular and Molecular Life Sciences* **65**, 1653–1668 (2008).
11. R. S. Cooper, E. R. Georgieva, P. P. Borbat, J. H. Freed, E. E. Heldwein, Structural basis for membrane anchoring and fusion regulation of the herpes simplex virus fusogen gB. *Nature Structural & Molecular Biology* **25**, 416–424 (2018).
12. S. C. Harrison, Viral membrane fusion. *Virology* **479-480**, 498–507 (2015).
13. A. V. Nicola, Herpesvirus Entry into Host Cells Mediated by Endosomal Low <scp>pH</scp>. *Traffic* **17**, 965–975 (2016).
14. K. Sathiyamoorthy, J. Chen, R. Longnecker, T. S. Jardetzky, The COMPLEXity in herpesvirus entry. *Current Opinion in Virology* **24**, 97–104 (2017).
15. M. Backovic, T. S. Jardetzky, Class III viral membrane fusion proteins. *Current Opinion in Structural Biology* **19**, 189–196 (2009).
16. D. Atanasiu, W. T. Saw, G. H. Cohen, R. J. Eisenberg, Cascade of Events Governing Cell-Cell Fusion Induced by Herpes Simplex Virus Glycoproteins gD, gH/gL, and gB. *Journal of Virology* **84**, 12292–12299 (2010).
17. J. S. McLellan, Neutralizing epitopes on the respiratory syncytial virus fusion glycoprotein. *Current Opinion in Virology* **11**, 70–75 (2015).
18. J. S. McLellan *et al.*, Structure-Based Design of a Fusion Glycoprotein Vaccine for Respiratory Syncytial Virus. *Science* **342**, 592–598 (2013).
19. J. S. McLellan *et al.*, Structure of RSV Fusion Glycoprotein Trimer Bound to a Prefusion-Specific Neutralizing Antibody. *Science* **340**, 1113–1117 (2013).

20. J. O. Ngwuta *et al.*, Prefusion F–specific antibodies determine the magnitude of RSV neutralizing activity in human sera. *Science Translational Medicine* **7**, 309ra162–309ra301 (2015).
21. R. W. Sanders *et al.*, HIV-1 neutralizing antibodies induced by native-like envelope trimers. *Science* **349**, aac4223–aac4223 (2015).
22. I. Rossey, J. S. McLellan, X. Saelens, B. Schepens, Clinical Potential of Prefusion RSV F-specific Antibodies. *Trends in Microbiology* **26**, 209–219 (2018).
23. H. M. Callaway *et al.*, Structure of the rabies virus glycoprotein trimer bound to a prefusion-specific neutralizing antibody. *Science Advances* **8**, eabp9151 (2022).
24. L. Zhong *et al.*, Targeting herpesvirus entry complex and fusogen glycoproteins with prophylactic and therapeutic agents. *Trends in Microbiology* **31**, 788–804 (2023).
25. R. S. Roark *et al.*, Prefusion structure, evasion and neutralization of HSV-1 glycoprotein B. *Nature Microbiology* **10**, 2966–2980 (2025).
26. B. Vollmer *et al.*, A nanobody specific to prefusion glycoprotein B neutralizes HSV-1 and HSV-2. *Nature*, (2025).
27. I. M. Backes, D. A. Leib, M. E. Ackerman, Monoclonal antibody therapy of herpes simplex virus: An opportunity to decrease congenital and perinatal infections. *Frontiers in Immunology* **13**, (2022).
28. M. D. Slein *et al.*, Effector functions are required for broad and potent protection of neonatal mice with antibodies targeting HSV glycoprotein D. *Cell Reports Medicine* **5**, 101417 (2024).
29. M. D. Slein *et al.* (Cold Spring Harbor Laboratory, 2025).
30. K. Wang *et al.*, Monoclonal Antibodies, Derived from Humans Vaccinated with the RV144 HIV Vaccine Containing the HVEM Binding Domain of Herpes Simplex Virus (HSV) Glycoprotein D, Neutralize HSV Infection, Mediate Antibody-Dependent Cellular Cytotoxicity, and Protect Mice. *Journal of Virology* **91**, e00411–00417 (2017).
31. N. Seyfizadeh *et al.*, Development of a highly effective combination monoclonal antibody therapy against Herpes simplex virus. *Journal of Biomedical Science* **31**, (2024).
32. M. Kuraoka *et al.*, A non-neutralizing glycoprotein B monoclonal antibody protects against herpes simplex virus disease in mice. *Journal of Clinical Investigation* **133**, (2023).
33. F. C. Bender *et al.*, Antigenic and Mutational Analyses of Herpes Simplex Virus Glycoprotein B Reveal Four Functional Regions. *Journal of Virology* **81**, 3827–3841 (2007).
34. C. Sun *et al.*, The structure of HSV-1 gB bound to a potent neutralizing antibody reveals a conservative antigenic domain across herpesviruses. *hLife* **2**, 141–146 (2024).
35. S. Pötzsch *et al.*, B Cell Repertoire Analysis Identifies New Antigenic Domains on Glycoprotein B of Human Cytomegalovirus which Are Target of Neutralizing Antibodies. *PLOS Pathogens* **7**, e1002172 (2011).
36. H.-J. Stellbrink *et al.*, Safety and efficacy of monoclonal antibody therapy in patients with chronic herpes simplex virus-2 genital infections: MATCH-2, a randomized double-blinded, parallel-group phase 2 multi-center trial. *Pharmacological Research* **221**, 107999 (2025).

37. A. Krawczyk *et al.*, Overcoming drug-resistant herpes simplex virus (HSV) infection by a humanized antibody. *Proceedings of the National Academy of Sciences* **110**, 6760–6765 (2013).
38. I. Setliff *et al.*, High-Throughput Mapping of B Cell Receptor Sequences to Antigen Specificity. *Cell* **179**, 1636–1646.e1615 (2019).
39. M. R. Sponholtz *et al.* (openRxiv, 2026).
40. M. R. Sponholtz *et al.*, Structure-based design of a soluble human cytomegalovirus glycoprotein B antigen stabilized in a prefusion-like conformation. *Proceedings of the National Academy of Sciences* **121**, (2024).
41. R. S. McCool *et al.*, Structure and immunogenicity of an engineered soluble prefusion-stabilized EBV gB antigen. *Nature Communications*, (2026).
42. N. T. Mori H, Shimizu H, Koube A. (2020), chap. US20200239549-A1.
43. Y. Liu *et al.*, Prefusion structure of human cytomegalovirus glycoprotein B and structural basis for membrane fusion. *Science Advances* **7**, eabf3178 (2021).
44. R. S. McCool *et al.*, Structure and immunogenicity of an engineered soluble prefusion-stabilized EBV gB antigen. *Nat Commun* **17**, 1197 (2026).
45. C. M. Ives *et al.*, Restoring protein glycosylation with GlycoShape. *Nature Methods* **21**, 2117–2127 (2024).
46. T. D. Szucs, K. Berger, D. N. Fisman, S. Harbarth, The estimated economic burden of genital herpes in the United States. An analysis using two costing approaches. *BMC Infectious Diseases* **1**, (2001).
47. S. Silva, H. H. Ayoub, C. Johnston, R. Atun, L. J. Abu-Raddad, Estimated economic burden of genital herpes and HIV attributable to herpes simplex virus type 2 infections in 90 low- and middle-income countries: A modeling study. *PLOS Medicine* **19**, e1003938 (2022).
48. K. Madavaraju, R. Koganti, I. Volety, T. Yadavalli, D. Shukla, Herpes Simplex Virus Cell Entry Mechanisms: An Update. *Frontiers in Cellular and Infection Microbiology* **10**, (2021).
49. D. C. Johnson, T. W. Wisner, C. C. Wright, Herpes Simplex Virus Glycoproteins gB and gD Function in a Redundant Fashion To Promote Secondary Envelopment. *Journal of Virology* **85**, 4910–4926 (2011).
50. L. Milojević *et al.*, Capturing intermediates and membrane remodeling in class III viral fusion. *Science Advances* **10**, (2024).
51. M. Kim, Z. Qiao, J. Yu, D. Montefiori, E. L. Reinherz, Immunogenicity of recombinant human immunodeficiency virus type 1-like particles expressing gp41 derivatives in a pre-fusion state. *Vaccine* **25**, 5102–5114 (2007).
52. D. W. Kulp *et al.*, Structure-based design of native-like HIV-1 envelope trimers to silence non-neutralizing epitopes and eliminate CD4 binding. *Nature Communications* **8**, 1655 (2017).
53. D. W. Kimberlin *et al.*, Safety and Efficacy of High-Dose Intravenous Acyclovir in the Management of Neonatal Herpes Simplex Virus Infections. *Pediatrics* **108**, 230–238 (2001).
54. H. M. Friedman *et al.*, Immune evasion properties of herpes simplex virus type 1 glycoprotein gC. *Journal of Virology* **70**, 4253–4260 (1996).
55. L. N. Akhtar *et al.*, Genotypic and Phenotypic Diversity of Herpes Simplex Virus 2 within the Infected Neonatal Population. *mSphere* **4**, (2019).

56. R. Manivanh, J. Mehrbach, D. M. Knipe, D. A. Leib, Role of Herpes Simplex Virus 1 γ34.5 in the Regulation of IRF3 Signaling. *Journal of Virology* **91**, (2017).
57. K. A. Rader, C. E. Ackland-Berglund, J. K. Miller, J. S. Pepose, D. A. Leib, In vivo characterization of site-directed mutations in the promoter of the herpes simplex virus type 1 latency-associated transcripts. *Journal of General Virology* **74**, 1859–1869 (1993).
58. M. R. Sponholtz *et al.*, Structure-based design of soluble prefusion-stabilized herpes simplex virus type 2 glycoprotein B antigens. *bioRxiv*, 2026.2001.2026.701809 (2026).
59. A. A. Abu-Shmais *et al.*, Antibody sequence determinants of viral antigen specificity. *mBio* **15**, (2024).
60. E. Alamyar, V. Giudicelli, P. Duroux, M.-P. Lefranc, paper presented at the Journées Ouvertes de Biologie, Informatique et Mathématiques, Montpellier, France, 2010–09–07 2010.
61. P. T. Wasdin *et al.*, Generation of antigen-specific paired-chain antibodies using large language models. *Cell* **188**, 7206–7221.e7216 (2025).
62. B. Abanades *et al.*, The Patent and Literature Antibody Database (PLAbDab): an evolving reference set of functionally diverse, literature-annotated antibody sequences and structures. *Nucleic Acids Research* **52**, D545–D551 (2024).
63. M. P. Lefranc *et al.*, IMGT(R), the international ImMunoGeneTics information system(R). *Nucleic Acids Research* **37**, D1006–D1012 (2009).
64. M. I. J. Raybould, A. Kovaltsuk, C. Marks, C. M. Deane, CoV-AbDab: the coronavirus antibody database. *Bioinformatics* **37**, 734–735 (2021).
65. H. Yoon *et al.*, CATNAP: a tool to compile, analyze and tally neutralizing antibody panels. *Nucleic Acids Research* **43**, W213–W219 (2015).
66. A. Kovaltsuk *et al.*, Observed Antibody Space: A Resource for Data Mining Next-Generation Sequencing of Antibody Repertoires. *The Journal of Immunology* **201**, 2502–2509 (2018).
67. M. I. J. Raybould *et al.*, Thera-SAbDab: the Therapeutic Structural Antibody Database. *Nucleic Acids Research* **48**, D383–D388 (2020).
68. P. Dudzic *et al.*, Conserved heavy/light contacts and germline preferences revealed by a large-scale analysis of natively paired human antibody sequences and structural data. *Communications Biology* **8**, (2025).
69. A. Bateman *et al.*, UniProt: the Universal Protein Knowledgebase in 2023. *Nucleic Acids Research* **51**, D523–D531 (2023).
70. D. N. Mastronarde, Automated electron microscope tomography using robust prediction of specimen movements. *Journal of Structural Biology* **152**, 36–51 (2005).
71. A. Punjani, J. L. Rubinstein, D. J. Fleet, M. A. Brubaker, cryoSPARC: algorithms for rapid unsupervised cryo-EM structure determination. *Nature Methods* **14**, 290–296 (2017).
72. H. Cao, T. Li, J. He, S. Huang, BPS2025 - EMReady2: A general model for improving cryo-EM and cryo-ET maps by heterogeneity-aware deep learning. *Biophysical Journal* **124**, 625a (2025).
73. A. Morin *et al.*, Collaboration gets the most out of software. *eLife* **2**, e01456 (2013).
74. J. Abramson *et al.*, Accurate structure prediction of biomolecular interactions with AlphaFold 3. *Nature* **630**, 493–500 (2024).
75. E. F. Pettersen *et al.*, <scp>UCSF ChimeraX</scp>: Structure visualization for researchers, educators, and developers. *Protein Science* **30**, 70–82 (2021).

76. P. Emsley, K. Cowtan, Coot: model-building tools for molecular graphics. *Acta Crystallographica Section D Biological Crystallography* **60**, 2126–2132 (2004).
77. D. Liebschner *et al.*, Macromolecular structure determination using X-rays, neutrons and electrons: recent developments in Phenix. *Acta Crystallographica Section D Structural Biology* **75**, 861–877 (2019).
78. T. I. Croll, ISOLDE: a physically realistic environment for model building into low-resolution electron-density maps. *Acta Crystallographica Section D Structural Biology* **74**, 519–530 (2018).
79. F. Sievers, D. G. Higgins, Clustal Omega for making accurate alignments of many protein sequences. *Protein Science* **27**, 135–145 (2018).

ACKNOWLEDGMENTS

We thank all members of the Georgiev laboratory and McLellan laboratory for their support and feedback. We thank David Flaherty, Olivia Murfield, Emma McLaughlin, and Brittany Matlock from the VUMC Flow Cytometry Shared Resource for their help with cell sorting. The VUMC Flow Cytometry Shared Resource is supported by the Vanderbilt Ingram Cancer Center (P30 CA68485) and the Vanderbilt Digestive Disease Research Center (DK058404). We thank Angela Jones, Jamie Roberson, and Latha Raju with the Vanderbilt Technologies for Advanced Genomics Core (VANTAGE) for providing technical assistance with library production and sequencing. VANTAGE is supported in part by CTSA (5UL1 RR024975-03), the Vanderbilt-Ingram Cancer Center (P30 CA68485), the Vanderbilt Vision Center (P30 EY08126), and NIH/NCRR (G20 RR030956). We thank Dr. Axel Brilot and Dr. Evan Schwartz at the Sauer Structural Biology Laboratory at UT Austin for assistance with cryo-EM data collection, which is supported in part by The University of Texas at Austin College of Natural Sciences and award RR160023 of the Cancer Prevention and Research Institute of Texas. The funders had no role in the conceptualization or execution of any studies or drafting of the manuscript.

National Institutes of Health grant R01AI175245 (ISG, PA, GJ, PTW, AAA)

National Institutes of Health grant R01AI176646 (NNM, DAL, MEA)

National Institutes of Health grant R01DK131070 (RHB)

Welch Foundation grant number F-0003-19620604 (JSM)

National Institutes of Health fellowship NIH F31DK141224 (LEB)

AUTHOR CONTRIBUTIONS

Conceptualization: PA, JK, NVJ, AAA, JSM, ISG

Investigation: PA, JK, NNM, PTW, GJ, LEB, NVJ

Supervision: MEA, DAL, RHB, JSM, ISG

Writing – original draft: PA, JK, JSM, ISG

Writing – review & editing: PA, JK, NNM, PTW, LEB, GJ, AAA, MDS, NVJ, RHB, DAL, MEA, JSM, ISG

COMPETING INTERESTS

PA, JK, NNM, DAL, MEA, JSM, and ISG are listed as inventors on patents filed describing the antibodies discovered here. ISG is listed as an inventor on patent applications for the LIBRA-seq technology. JSM is listed as an inventor on a patent application describing prefusion-stabilized HSV-2 gB proteins. ISG is a co-founder of AbSeek Bio. ISG has served as a consultant for Sanofi. The Georgiev laboratory at VUMC has received unrelated funding from Merck and Takeda Pharmaceuticals. The Ackerman laboratory at Dartmouth has received unrelated funding from Be Bio and Moderna.

DATA, CODE, AND MATERIALS AVAILABILITY

All data are available in the main text or the supplementary materials.

MAIN FIGURES

A

Name	Native Isotype	VH Gene	CDRH3	CDRH3 Length	VL Gene	CDRL3	CDRL3 Length	LIBRA-seq Score (LSS) HSV-2 Prefusion gB	LIBRA-seq Score (LSS) HSV-2 Postfusion gB
1-9	IGHG1	IGHV3-74	TRSSVSGTFPFDF	13	IGLV3-21	QVWDSNSDHVV	11	1.42	1.13
1-10	IGHG1	IGHV5-51	ARQGFFYNGAGTYSQAFDY	19	IGKV3-20	QLYGDSPTWT	10	1.37	1.02
1-11	IGHG3	IGHV3-7	ARDAFYLDLDH	11	IGLV1-40	QSFDSSLSGRV	11	1.28	1.54
1-12	IGHG1	IGHV5-51	ARQGYFYYGGGTYSQAFDY	19	IGKV3-20	QLYGNSPTWT	10	1.33	1.01
1-13	IGHG1	IGHV3-23	TKADRMATRLYYFDH	15	IGKV1-5	QQYNSYSYT	9	1.31	0.40
1-14	IGHG1	IGHV3-30	GRVARQFLENVYVDM	15	IGKV3-15	QHYHTWPPS	9	1.24	-1.03
1-15	IGHG1	IGHV5-51	MAGGYYDSGNL	11	IGKV2-28	MQVLQTPLT	9	1.05	0.76
1-16	IGHG1	IGHV1-2	ARLLGFKKFYDNSGYHTP	18	IGLV1-40	QSYDYRLSGWV	11	0.24	1.73
1-17	IGHG1	IGHV1-2	ARDLARTDEIVGPFKWFDP	19	IGLV1-40	QSYDHSLGGSV	11	0.01	1.62
3-5	IGHG1	IGHV4-4	ARDSGTYFDY	10	IGLV2-14	SSHSSSSTRVV	11	1.36	-1.19
3-6	IGHG1	IGHV3-30	ARDAMWEWSGGAGYYRFYGMDV	22	IGLV1-44	GAWDDSQSGFFV	12	1.23	-1.19
3-7	IGHG1	IGHV3-53	ARVGGGTSGPLDY	13	IGLV3-21	QVWDRSSGHLV	11	1.34	1.15
3-8	IGHG1	IGHV3-73	ARHATDSASGSFDF	14	IGLV3-21	QVWDNSSDQGV	11	1.25	1.12
3-11	IGHG2	IGHV4-30	ARTGGCSGVNCPSGYTDF	18	IGLV3-21	QVWDSGQV	8	1.26	1.12
5-12	IGHG1	IGHV1-18	ARGGGSAALPHAFDI	15	IGKV1-5	QQYHDFPWT	9	2.21	1.15
5-13	IGHG1	IGHV3-7	ARDTLMTIDY	10	IGLV2-8	SSYAGSNNLYV	11	2.63	-0.37
5-14	IGHG1	IGHV1-46	ARSVMATVPYDY	12	IGKV1-39	QQSYNTLPIT	10	1.63	0.54
5-15	IGHG1	IGHV3-23	ARDELPSTVFDY	12	IGLV4-69	QSWGKGIYAV	10	1.56	0.83
5-16	IGHG1	IGHV4-59	ARGRLTATIPVDH	13	IGKV1-33	QQYDGLPYT	9	1.95	0.59
5-18	IGHM	IGHV4-39	ARVGGLTTVVTPVDY	15	IGKV1-5	QHYNSYSGT	9	3.14	-1.65
5-20	IGHA1	IGHV4-31	ASDLGGIHD	9	IGKV1-39	QQSDSVPIT	9	0.30	1.13
5-21	IGHA1	IGHV1-2	ARELFREDYYDKIGCFDP	18	IGLV1-40	QSYDISLSGSV	11	0.23	1.47

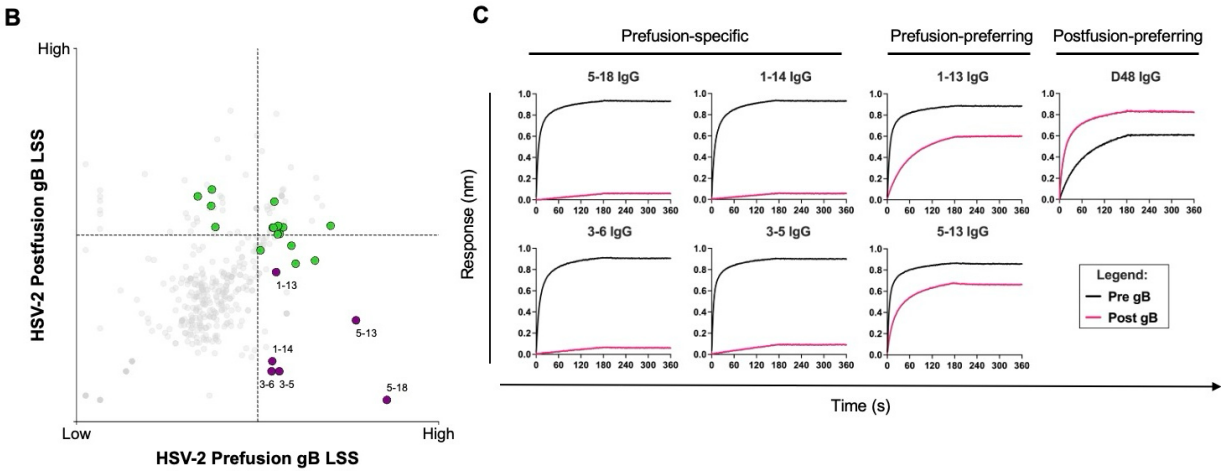

Fig 1. Identification and characterization of HSV-2 prefusion-specific human antibodies. (A) Sequence properties of HSV-2 gB antibodies identified by LIBRA-seq. The complementarity-determining region (CDR) sequences and lengths for each antibody are shown at the amino acid level. LIBRA-seq scores (LSS) for the selected antibodies to HSV-2 pre- and postfusion gB antigens are shown as a heat map from –2 (tan) to 0 (white) to 2 (purple); scores outside of this range are shown as the minimum and maximum values. **(B)** LIBRA-seq scores for each recovered B cell are plotted, with cutoffs set at an LSS of 1. Antibodies encoded by B cells colored in purple were selected for experimental validation. The remaining 22 selected antibodies are colored green. **(C)** BLI sensorgrams for immobilized IgGs binding to prefusion-stabilized HSV-2 gB (black) or postfusion HSV-2 gB (pink).

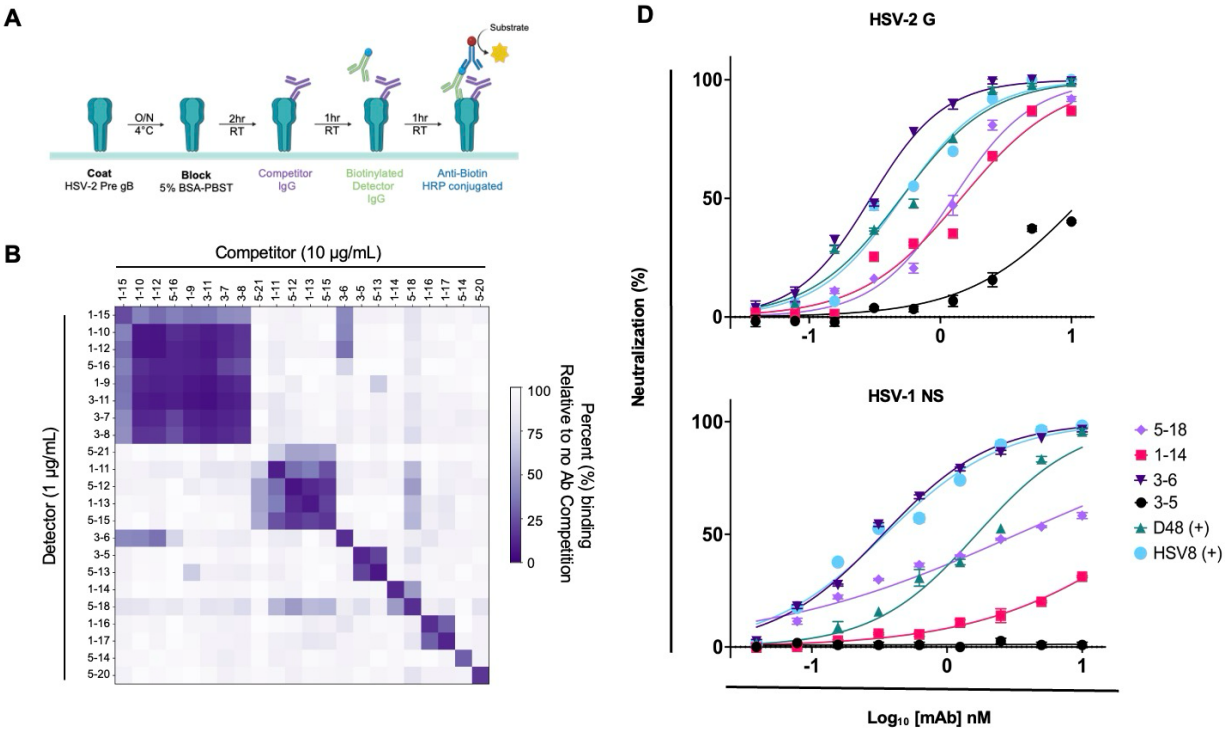

C

Specificity	Fab	HSV-2 Prefusion gB		HSV-1 Prefusion gB	
		*K*d (nM)	Dissociation Rate Constant (k_{off})	*K*d (nM)	Dissociation Rate Constant (k_{off})
Prefusion-specific	5-18	0.20	1.8×10^{-4} s^{-1}	40.00	2.3×10^{-3} s^{-1}
	1-14	0.03	1.2×10^{-5} s^{-1}	0.12	1.1×10^{-5} s^{-1}
	3-6	0.12	5.3×10^{-5} s^{-1}	0.08	7.5×10^{-5} s^{-1}
	3-5	0.15	8.2×10^{-5} s^{-1}	0.04	4.3×10^{-5} s^{-1}
Prefusion-preferring	1-13	0.11	9.9×10^{-5} s^{-1}	3.20	1.1×10^{-4} s^{-1}
	5-13	0.17	6.1×10^{-5} s^{-1}	0.21	1.1×10^{-4} s^{-1}

E

	1-14	3-5	3-6	5-18	D48 (+)	HSV8 (+)
HSV2-G	1.44	12.32	0.29	1.25	0.50	0.51
HSV1-NS	>	>	0.34	3.30	1.66	0.35

> 15 nM
5 - 15 nM
1.1 - 5 nM
< 1 nM

Fig 2. Binding and neutralization of prefusion-specific gB antibodies. (A) ELISA-based antibody-antibody binding competition assay (schematic created using Biorender.com). **(B)** The percentage of binding remaining in the presence of a competitor mAb is shown for each mAb, with darker colors corresponding to stronger competition between the given pair of mAbs. Dark purple clusters indicate a group of mAbs targeting overlapping epitopes on the HSV-2 prefusion gB antigen. **(C)** Equilibrium dissociation constants (Kd) and dissociation rate constants (kd) of gB Fabs binding to immobilized HSV-2 prefusion gB on Ni2+-NTA biosensors. **(D)** Neutralization profiles of gB-specific mAbs against HSV-2 G and HSV-1 NS strains detected by a plaque reduction assay. **(E)** Neutralization midpoint concentration (IC50) summary heatmap, with strong neutralization of HSV-2 G and HSV-1 NS (< 1 nM) shown in dark purple and weak/non-neutralizing (> 15 nM) shown in light purple. Calculated by non-linear regression analysis using GraphPad Prism software.

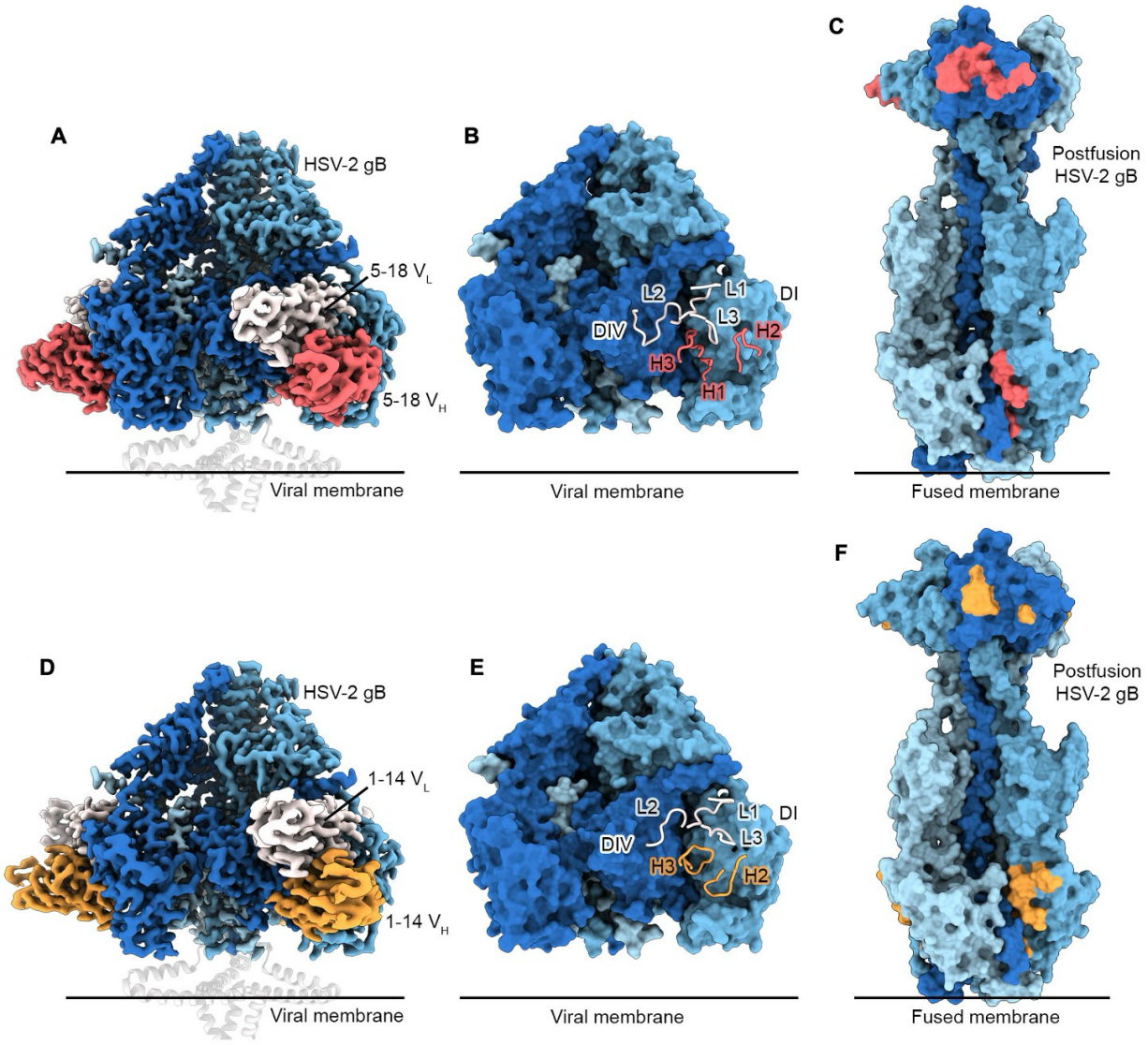

Fig 3. Fabs 5-18 and 1-14 recognize prefusion-specific quaternary epitopes spanning domains I and IV. (A) Cryo-EM map side view of Fab 5-18 bound to the HSV-2 prefusion gB trimer. The 5-18 VH is colored red, and the VL is colored white. Each prefusion gB protomer is colored a different shade of blue. The MPR and TM regions from PDB ID: 9Q9L are shown as transparent helices, and a horizontal black line indicates the approximate position of the viral membrane. **(B)** Side view of prefusion HSV-2 gB depicted as a molecular surface with the 5-18 CDRs depicted as ribbons. Domain I (DI) and domain IV (DIV) are labeled on gB. **(C)** Side view of postfusion HSV-2 gB (PDB ID: 8RH2) shown as a molecular surface with the 5-18 epitope colored red. The fused membrane is indicated by a horizontal black line. **D, E, and F,** are the same as **A, B,** and **C,** but depict the Fab 1-14 complex, CDRs, and epitope.

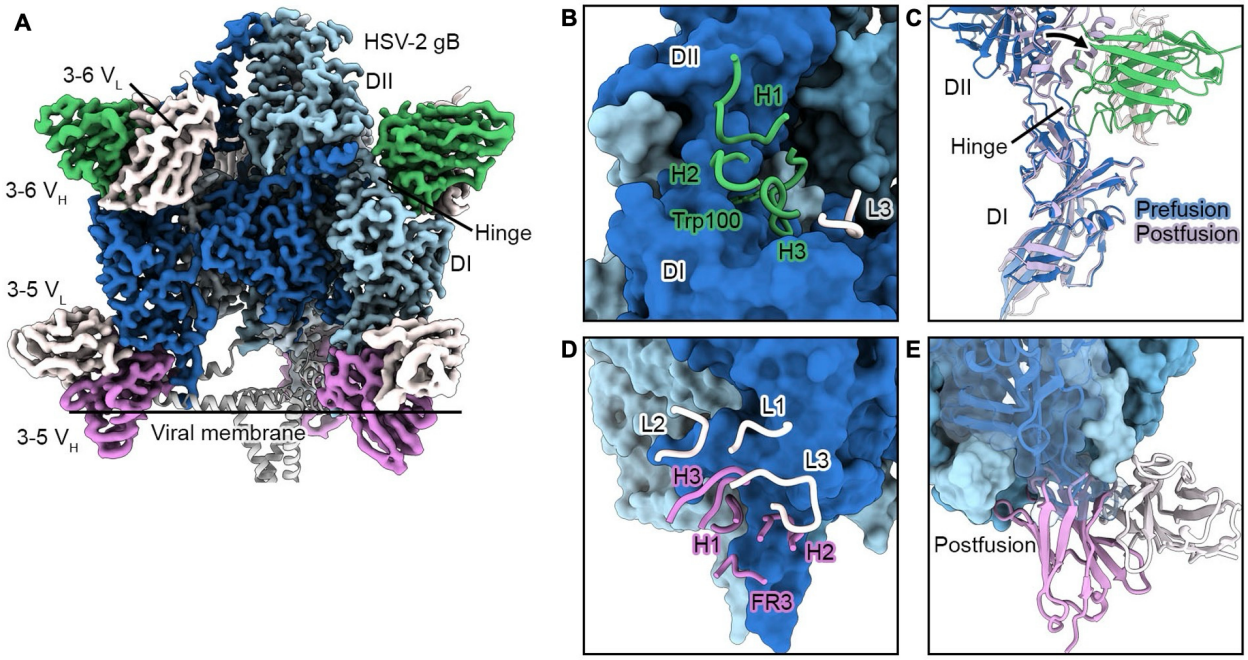

Fig 4. Antibodies 3-6 and 3-5 bind distinct prefusion-specific epitopes located within a single protomer. (A) Cryo-EM map side view of Fabs 3-6 and 3-5 bound to the HSV-2 prefusion gB trimer. The 3-6 VH is colored green, the 3-5 VH is colored magenta, and both VLs are colored white. Each prefusion gB protomer is colored a different shade of blue. The MPR and TM regions from PDB ID: 9Q9L are shown as white helices, and a horizontal black line indicates the approximate position of the viral membrane. **(B)** Magnified view of prefusion HSV-2 gB depicted as a molecular surface with the 3-6 CDRs depicted as ribbons. Domain I (DI) and domain II (DII) are labeled on gB. The sidechain of Trp100 in the HCDR3 (H3) is shown as sticks. **(C)** Superimposition of DI from the 3-6-bound prefusion gB monomer and a monomer from postfusion gB (PDB ID: 8RH2) showing the rearrangement of DII (indicated with a black arrow) that blocks Fab 3-6 binding. **(D)** Magnified view of prefusion HSV-2 gB depicted as a molecular surface with the 3-5 CDRs and framework 3 (FR3) region depicted as ribbons. **(E)** Magnified view of a superposition of the postfusion gB trimer (PDB ID: 8RH2) and Fab 3-5, with one protomer surface rendered transparent and the chain shown as ribbons. In the postfusion conformation, gB cannot bind Fab 3-5 due to numerous clashes.

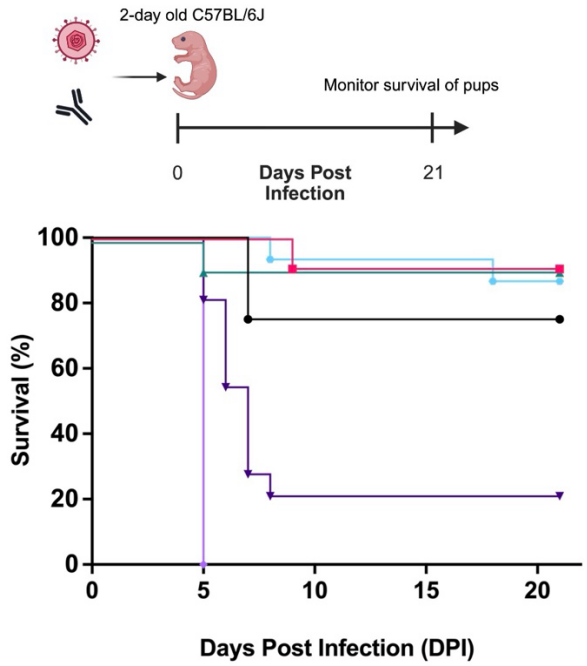

mAb	Overall Survival Proportions (%)	P-value compared to VRC01 control
3-6	90.91	0.0002
5-18	75.00	0.0001
1-14	20.00	0.0020
D48	86.67	<0.0001
HSV8	90.91	0.0009
VRC01	0.00	-

Fig 5. Prefusion-specific gB antibodies protect from viral challenge in a neonatal mouse model. Overall survival of 2-day old C57BL/6J mice infected intranasally with 500 plaque-forming units (PFU) of HSV-2-CNS11 and treated intraperitoneally with 80 µg monoclonal antibody IgG1 (3-6: n=11, 5-18: n=12, 1-14: n=15, D48: n=15, HSV8: n=11, VRC01: n=9) as shown on the experimental timeline (schematic created using Biorender.com). Statistical significance between the negative control VRC01 mAb and experimental antibodies was calculated by log(rank) (Mantel-Cox) test. Summary table with the overall survival proportions for each experimental group at 21 days post-infection as determined by the survival analysis Kaplan-Meier test.

MATERIALS AND METHODS

Cells and viruses

FreeStyle 293F cells (Gibco), Expi293 cells (Gibco), Vero cells (ATCC, cat. no. CCL-81), HEp-2 cells (ATCC, cat. no. CCL-23), and HEK293T cells (ATCC, cat. no. CRL-3216) were cultured according to vendor instructions. Virus strains used in this study included HSV2-G (*53*), HSV1-NS (*54*), and HSV2-CNS11 (*55*). For virus propagation, Vero cells were used to prepare viral stocks as described previously (*56, 57*).

Mice

C57BL/6J (RRID:IMSR_JAX:000664) mice were either purchased from The Jackson Laboratories or bred in animal facilities at Dartmouth College in accordance with Institutional Animal Care and Use Committee protocols (Dartmouth College IACUC protocol 2151).

Human blood sample collection and preparation

Prospective blood collection and peripheral blood mononuclear cell (PBMC) isolation from HSV-2 positive donors were procured from BioCollections Worldwide, Inc. (Miami, FL) and certified by BioPlex 2200 HSV-1 & HSV-2 IgG kit on the BioPlex 2200 System. Healthy donor PBMCs with no recorded history of prior infection were purchased commercially from StemCell Technologies (catalog number 70025.3). Samples arrived frozen and were stored at -135 °C until use.

HSV gB expression and purification

HSV-1 gB ectodomain (Strain KOS; Uniprot: P06437, residues 31–725) was engineered in both postfusion and prefusion-stabilized forms using the same prefusion-stabilizing substitutions as the HSV-2 gB constructs (Strain HG52; Uniprot: P06763, residues 23–731; postfusion gB-B1 and

prefusion-stabilized gB-O3)(*58*). For HSV-1 prefusion gB, the N-terminal disordered region (residues 32–78) was truncated to improve expression, an interprotomer disulfide bond (T243C/E679C) and two proline substitutions (S688P and T669P) were introduced to stabilize the prefusion conformation, and substitutions H172N and Y174T were incorporated to reduce aggregation (**fig. S5**). All constructs were transiently expressed in FreeStyle 293F cells using polyethylenimine (PEI) transfection reagent. Cultures were maintained at 37 °C and 8% CO_2, and the media were harvested 6 days post-transfection. The supernatants were filtered through a 0.22 μm membrane and loaded onto Strep-Tactin 4Flow resin (IBA Lifesciences) by gravity. After washing with 100 mM Tris-HCl pH 8.0, 150 mM NaCl, and 1 mM EDTA, the bound proteins were eluted with 100 mM Tris-HCl pH 8.0, 150 mM NaCl, 1 mM EDTA, and 50 mM biotin (IBA Lifescience). The elution fractions were incubated overnight at 4 °C with 5% (w/w) His-tagged HRV3C protease to remove purification tags. The samples were then purified by size-exclusion chromatography (SEC) using a Superose 6 Increase 10/300 GL column (Cytiva) equilibrated in phosphate-buffered saline (PBS).

Oligonucleotide barcodes

Oligonucleotides composed of a 15 bp antigen barcode were used with sequence modifications to anneal to the template switch oligo on the 10x bead-delivered oligos and truncated TruSeq small RNA read 1 sequence in the following structure: 5′ CCTTGGCACCCGAGAATTCCANNNNNNNNNNNNNCCCATATAAGA∗A∗A-3′, where N represent the antigen barcode. For each antigen, we used the following barcode sequences: HSV-2 gB-G3 prefusion (GACAAGTGATCTGCA), HSV-2 gB B1 postfusion (AACCCACCGTTGTTA), HCMV gB C7 prefusion (CAGTAGATGGAGCAT), HCMV gB base postfusion (ATCGTCGAGAGCTAG), EBV gB C3-GT prefusion (TGTGTATTCCCTTGT),

EBV gB base postfusion (GCTCCTTTACACGTA), HIV BG505 gp140 V9.3 SOSIP (TCACAGTTCCTTGGA), and influenza HA NC99 (GGTAGCCCTAGAGTA). Oligos were ordered from Sigma-Aldrich and IDT with a 5′ amino modification and HPLC purified.

Antigen labeling with DNA oligonucleotide barcodes

For each antigen, the unique DNA barcodes were directly conjugated using SoluLINK Protein-Oligonucleotide Conjugation kit (Vector Labs, S-9011) according to the kit's protocol. Each antigen was biotinylated using EZ link (Thermo), desalted and modified with S-HyNic. The 4FB-modified DNA barcodes were directly conjugated to the biotinylated antigen with S-HyNic to create a stable bond between the protein and oligonucleotide. The antigen-oligonucleotide conjugate concentrations were determined using a bicinchoninic acid (BCA) assay, and the HyNic molar substitution ratios of each antigen-oligonucleotide conjugate were determined using a NanoDrop according to the SoluLINK protocol instructions. Excess oligonucleotides were removed from the protein-oligonucleotide conjugates using an AKTA FPLC and were subsequently verified using SDS-PAGE and silver stain. The optimal amounts of antigen-oligonucleotide conjugates to be used in antigen-specific B cell sorting were then determined through flow cytometry titration experiments on cell lines expressing BCRs of known specificities.

Antigen-specific B cell sorting

PBMCs were thawed and counted using Trypan Blue viability stain. Cells were washed with a solution of Dulbecco's phosphate-buffered saline (DPBS) supplemented with 0.1% bovine serum albumin (BSA). Samples were resuspended in DPBS-BSA and stained with cell markers: CD14 (BD, cat no. 301819, clone M5E2, 1:10), Ghost Dye Red 780 Viability (Cell Signaling Technology, cat no. 18452S, 1:1000), CD3 (Cytek Biosciences, cat no. 35-0037, clone OKT3), CD19 (BD, cat no. 563036, clone SJ25C1), and IgG (BD, cat no. 551497, clone G18 145). Samples were

resuspended in DPBS-BSA before surface staining for 30 min. Additionally, antigen-oligonucleotide conjugates were incorporated into the stain. After 30 min incubation in the dark at room temperature, cells were washed three times with DPBS-BSA at 300g for 5 min. Next, the samples were incubated for 15 min at room temperature with Streptavidin-PE (Invitrogen, cat no. S866) to label cells with bound antigen. The cells were again washed three times with DPBS-BSA, resuspended in DPBS, and sorted by FACS. Antigen-positive B cells were bulk sorted and sequenced at Vanderbilt Technologies for Advanced Genomics (VANTAGE) at an appropriate target concentration for 10X Genomics library preparation and subsequent sequencing. FACS data were analyzed using FlowJo (BD Biosciences).

Sample and library preparation for sequencing

Single-cell suspensions were processed using the Chromium Controller microfluidics device (10X Genomics) and B cell Single Cells V(D)J solution as per the manufacturer's instructions. The aim was to capture 10,000 B cells per 1/8 10X cassette. Slight modifications were made to intercept, amplify, and purify the antigen barcode libraries, as previously described (*59*).

Sequence processing and bioinformatics analysis

For bioinformatic processing of the LIBRA-seq sequencing reads, we followed our established pipeline, which takes paired-end FASTQ files of oligonucleotide libraries as input. This pipeline processes and annotates reads for cell barcodes, unique molecular identifiers (UMIs) and antigen barcodes, resulting in a cell-barcode and antigen-barcode UMI count matrix (*38*). B cell receptor contigs and antigen-barcode libraries were processed using CellRanger 3.1.0 (10x Genomics) with GRCh38 Human V(D)J 7.0.0 as reference. From the BCR sequencing, 8,467 functional paired heavy- and light-chain sequences were recovered. B cell receptor contigs were aligned to IMGT reference genes using High-V Quest (*60*).

Antibody expression and purification

Variable heavy and light genes were inserted into custom plasmids that encode the constant region for the human IgG1 heavy chain and respective lambda and kappa light chains (Genscript). The antibodies were expressed in Expi293 cells by co-transfecting heavy chain and light chain expression plasmids using PEI or Expifectamine transfection reagent (Thermo Fisher Scientific) and cultured for 4–5 days. Cultures were harvested and centrifuged, and supernatant was filtered through 0.45 μm Nalgene Rapid Flow Disposable Filter Units with PES membrane. The filtered supernatant was run over a column containing Protein A agarose resin that was equilibrated with PBS. The column was washed with PBS, and then the antibodies were eluted with 100 mM glycine-HCl at pH 2.7 directly into a 1:10 volume of 1 M Tris-HCl pH 8.0. Eluted antibodies were buffer exchanged into PBS using Amicon Ultra centrifugal filter units, centrifuging and topping off three times with PBS, and finally concentrated. The antibodies were analyzed by SDS-PAGE. Antibody plasmids were sequenced to confirm the expected heavy and light chains.

Indirect enzyme-linked immunosorbent assay (ELISA)

For indirect ELISA assays, maxisorp 96-well flat-bottomed plates (Thermo Fisher Scientific) were coated with recombinant gB antigen at 2 μg mL^{-1} in PBS overnight at 4 °C. Subsequent washes were performed with PBS-T (PBS supplemented with 0.05% v:v Tween20 (Millipore-Sigma)). Blocking was performed in 5% BSA in PBS-T for 2 h at room temperature and then washed three times with PBS-T. Primary antibodies were serially diluted 1:5 in 1% BSA in PBS-T with a starting concentration of 10 μg mL^{-1} and incubated at room temperature for 1 h, washed, and detected via a horseradish peroxidase-conjugated anti-mouse IgG secondary diluted 1:10,000 (Jackson ImmunoResearch). One-step TMB-ELISA substrate solution (Thermo Fisher Scientific) was

added to develop for 5 min and quenched with 1 N sulfuric acid. Absorbance at 450 nm (A_{450}) was measured on a microplate reader. ELISAs were performed in technical and biological duplicates.

Antibody competition ELISA

For competition ELISA assays, maxisorp 384-well microtiter plates (Thermo Fisher Scientific) were coated with recombinant gB antigen at 2 µg/mL in PBS overnight at 4 °C. Subsequent washes were performed three times with PBS-T. Blocking was performed in 5% BSA in PBS-T for 2 h at room temperature, followed by three washes with PBS-T. Primary competitor antibodies at 10 µg/mL were added to wells incubated for 1 h at room temperature. Without washing off the competitor antibody, a biotinylated preparation of antibodies was added to wells with primary antibody at a concentration of 1 µg/mL and incubated for 1 h at room temperature. Plates were washed three times with PBS-T and bound antibodies were detected via a horseradish peroxidase-conjugated mouse anti-biotin secondary diluted 1:4,000 (SouthernBiotech). One-step TMB-ELISA substrate solution (Thermo Fisher Scientific) was added, incubated for 5 min, and quenched with 1 N sulfuric acid. Absorbance at 450 nm (A_{450}) was measured on a microplate reader. The A_{450} signal obtained for binding of the biotin-labelled reference antibody in the presence of the unlabeled tested antibody was expressed as a percentage of the binding of the reference antibody alone. Competition ELISAs were performed in technical and biological duplicates.

Prefusion specificity measurement

Bio-layer interferometry (BLI) experiments were conducted on an OctetRED96e instrument (Sartorius) at 21°C with a shaking speed of 1000 rpm. For determination of prefusion specificity, HSV-2 gB-specific IgG antibodies were immobilized onto anti-human IgG Fc Capture (AHC) biosensors (Sartorius) to a response level of approximately 1.0 nm in HBS-EP buffer (10 mM

HEPES pH 7.4, 150 mM NaCl, 3 mM EDTA, 0.05% v/v surfactant P20) supplemented with 0.1 % w/v BSA. Loaded sensors were then dipped into wells containing 200 nM of HSV-2 or HSV-1 prefusion-stabilized gB or postfusion gB for 180 s (association phase), followed by 180 s of dissociation. Reference sensors were incubated in buffer alone under identical conditions. Data were reference-subtracted and analyzed using the Octet Analysis Studio (v13.0, Sartorius).

Public antibody analysis

Prefusion-specific gB mAbs (1-14, 5-18, 3-5, 3-6) and prefusion-preferring gB mAbs (1-13, 5-13) were compared against a database of previously published antibodies consisting of 1.7 million paired antibody sequences. This database consists of a previously curated dataset (*61*), expanded with antibodies from public databases (*62-69*). In comparing antibody pairs, V gene paralogues were treated as the same, and CDR3 identity was calculated by employing the Levenshtein distance metric, measuring the difference between amino acid sequences and dividing it by the length of the longer CDR3 region in the pair to obtain sequence identity. Scatterplots in **fig. S3A** depict these pairs of antibodies.

Affinity measurement

For kinetics analyses, HSV-2 IgGs containing an HRV3C protease cleavage site engineered between the CH1 and CH2 domains of the heavy chain were incubated with 5% (w/w) His-tagged HRV3C protease at 4°C overnight. The reaction mixtures were then passed over Protein A and Ni-NTA resins to remove the cleaved Fc fragment and excess protease. The resulting Fabs were purified by SEC on a Superdex 200 Increase column (Cytiva) equilibrated in PBS. Purified soluble HSV-2 and HSV-1 prefusion-stabilized gB bearing a C-terminal 8xHis-tag were immobilized onto Ni-NTA biosensors (Sartorius) to a response level of approximately 0.7–0.8 nm in HBS-P buffer (10 mM HEPES pH 7.4, 150 mM NaCl, 0.005% v/v Surfactant P20) with 20 mM imidazole and

0.1% w/v BSA. After establishing a 180s baseline, the immobilized HSV-2 and -1 gB sensors were dipped into wells containing two-fold serial dilutions of Fabs. Sensors immobilized with gB proteins were run in parallel using buffer-only as a reference control. Dissociation was monitored for 600 s by transferring sensors into buffer-only wells. All data were reference-subtracted and globally fit to a 1:1 binding model using the Octet Analysis Studio (v13.0, Sartorius).

Cryo-EM sample preparation and data collection

Purified HSV-2 prefusion-stabilized gB was mixed in PBS to a final concentration of 4.0 mg mL^{-1} with 1.2-fold molar excess of Fabs 5-18, 1-14, or a combination of 3-5 and 3-6. Complexes were incubated for 30 min at 4 °C before adding 10X CMC CHAPS (VitroEase™ Buffer Screening Kit, Thermo Fisher Scientific) to a final concentration of 0.25X CMC. Immediately after CHAPS addition, 3.0 µL of sample was applied to UltrAuFoil R1.2/1.3 grids (Electron Microscopy Sciences) that had been glow-discharged using a PELCO easiGlow (Ted Pella) for 30 s at 20 mA. Grid vitrification was performed using a Vitrobot Mark IV (Thermo Fisher Scientific) operated at 4 °C in 100% humidity. A blot force of 8 was applied for 6 s to remove excess liquid before plunge-freezing the grids into liquid ethane. For data collection, 2,553 movies for the Fab 1-14 complex, 2,551 movies for the 5-18 Fab complex, and 3,060 movies for the Fab 3-5/Fab 3-6 complex were collected from single grids using a Glacios TEM (Thermo Fisher Scientific) equipped with a Falcon 4 detector (Thermo Fisher Scientific). Data for the 1-14 and 1-15 complexes were acquired at a 30° stage tilt, whereas data for the 3-5/3-6 complex were collected without tilt. All movies were recorded using SerialEM v4.0.10 automation software (*70*). Movies were acquired at a calibrated pixel size of 0.933 Å/pixel (total dose: 49 $e^{-}/Å^{2}$). Additional details about data collection parameters are summarized in **Table S4.**

Cryo-EM processing and structure determination

Motion correction, CTF estimation, and particle picking were performed using CryoSPARC Live. All subsequent image processing steps were performed in CryoSPARC v4.7.1 and v5.0.0-privatebeta.3 (*71*). Briefly, particles underwent two rounds of *ab initio* reconstruction and heterogeneous refinement, followed by re-extraction at 384 px. Multiple rounds of non-uniform refinements with optimized parameters were then performed to improve resolution, followed by reference-based motion correction (**fig. S8, fig. S9 and fig. S12**). For the Fabs 3-5 and 3-6 complex, 3D classification was performed (**fig. S12**). Final map sharpening was performed using EMReady v2.2.2 (*72*) within the SBgrid environment (*73*). Initial models were generated by combining the HSV-2 prefusion-stabilized gB structure (*39*) with Alphafold3-predicted models of the variable regions of 5-18, 1-14, 3-5, and 3-6, produced by inputting their VH and VL sequences (https://alphafoldserver.com) (*74*). The highest-confidence output model was docked into the refined cryo-EM map via ChimeraX (*75*). Missing residues were manually built in Coot (*76*), and structures were interactively refined using a combination of Phenix (*77*), Coot, and ISOLDE (*78*). N-acetyl-glucosamine (NAG) and β-mannose (BMA) were added to glycosylation sites and refined using ChimeraX and ISOLDE. Antigen-antibody interfaces and buried surface areas were analyzed using the PDBe PISA service (European Bioinformatics Institute; http://www.ebi.ac.uk/pdbe/prot_int/pistart.html) and ChimeraX. Secondary structure elements were derived from the HSV-2 gB structure in complex with Fabs 3-6 and 3-5, and plotted alongside sequence alignments of HSV-1 and HSV-2 gB generated using the UniProt Clustal Omega server (*79*).

Plaque reduction neutralization test

Serial dilutions of mAbs were incubated with 75–160 plaque-forming units (PFU) of HSV1-NS or 65–120 PFU of HSV2-G for 1 h at 37 ºC and 5% CO_2. This mixture was added to a confluent layer

of Vero cells in 6-well plates and incubated for 1 h at 37 ºC and 5% CO_2, with shaking every 15 minutes, after which a 1:1 methylcellulose:media overlay was added. The plates were then incubated for 44 to 48 h at 37 ºC and 5% CO_2. Cells were fixed with a 1:1 ethanol:methanol solution for 30 min prior to staining with 12% Giemsa for 24 to 48 h. The stain was then removed, and plaques were counted to determine the extent of neutralization relative to virus-only controls.

Intracellular and extracellular flow cytometric analysis

HEp-2 and HEK293T cell lines were harvested for flow cytometry staining. Cells were incubated with Alexa Fluor 700 NHS ester (succinimidyl ester) (Thermo Fisher Scientific) prior to fixation/permeabilization to enable viability assessment. For extracellular staining, cells were incubated on ice with 25 µg/mL unlabeled experimental and control IgG mAbs diluted in flow cytometry staining buffer, or flow cytometry staining buffer alone (secondary controls). Cells were washed, and rat anti-human IgG Fc-PE/Cy7 (Biolegend cat no. 410721, clone M1310G05, 1:1500) was used to detect human IgG mAbs. For intracellular staining, cells were fixed and permeabilized using the BD Cytofix/Cytoperm kit, followed by incubation with 25 µg/mL experimental or control mAbs diluted in the kit perm/wash buffer per kit instructions. Cells were washed, and rat anti-human IgG Fc-PE/Cy7 (Biolegend cat no. 410721, clone M1310G05, 1:1500) was diluted in perm/wash buffer and used to detect human IgG mAbs. All cells were resuspended in 1% paraformaldehyde, 2 mM EDTA in PBS and stored at 4 °C prior to acquisition on a BD Biosciences LSR Fortessa flow cytometer. Data were analyzed using FlowJo software (BD Biosciences). Gating strategies and IgG^+ plots can be found in **fig. S7.**

Survival study in a neonatal mouse model

Two-day-old C57BL/6J pups under 1% isoflurane anesthesia were treated with 80 µg of mAb in a 20 µL volume intraperitoneally (i.p.) using a 25 µL Hamilton syringe and then immediately

challenged intranasally (i.n.) with 500 PFU of HSV2 CNS11 in a 5 µL volume and monitored for survival for 21 days post-infection. Survival endpoints were defined in accordance with the criteria specified in the IACUC protocol (excessive morbidity such as hunching, spasms and/or paralysis and/or >10% weight loss from the previous measurement). All animal procedures were performed following approval by Dartmouth's Institutional Animal Care and Use Committee and in accordance with Dartmouth's Center for Comparative Medicine and Research policies.

Statistical methods

All statistical analyses were performed using GraphPad Prism version 9.0.0. Results of the challenge study were graphed as a cumulative Kaplan-Meier survival curve, and comparisons between groups were performed using a log-rank (Mantel-Cox) test. *In vitro* neutralization curves were generated by fitting data points using a variable slope and a four-parameter regression curve (best-fit method). ELISA data were analyzed using variable slope and a four-parameter regression curve, with area under the curve (AUC) reported from log-transformed values. The number of replicates per experiment is indicated in the figure legends. No data or experiments were excluded unless there were technical issues with the experiment, and outliers were not excluded. Exact P values are denoted in the figures.

SUPPLEMENTAL FIGURES

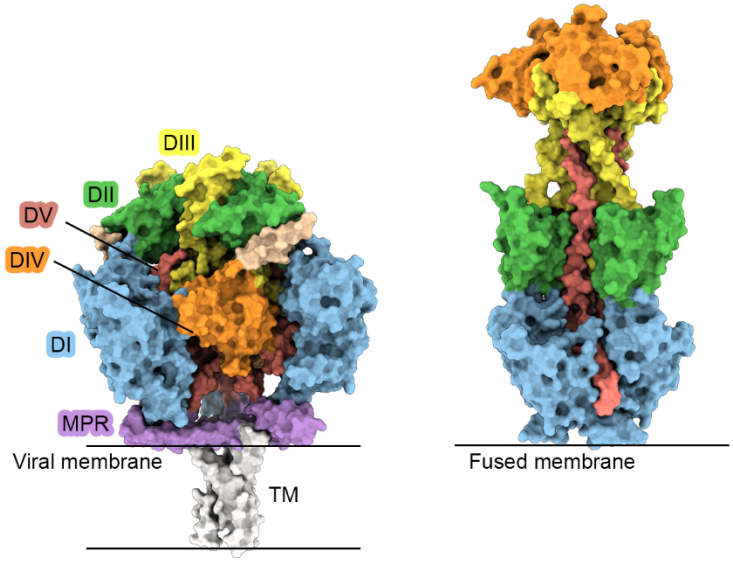

Fig. S1. Structural comparison of prefusion and postfusion gB. Side views of prefusion (PDB ID: 9Q9L) and postfusion (PDB ID: 9IH8) HSV-2 gB are shown as molecular surfaces. Domain (D) I is colored blue, DII is colored green, DIII is colored yellow, DIV is colored orange, DIV is colored red, and

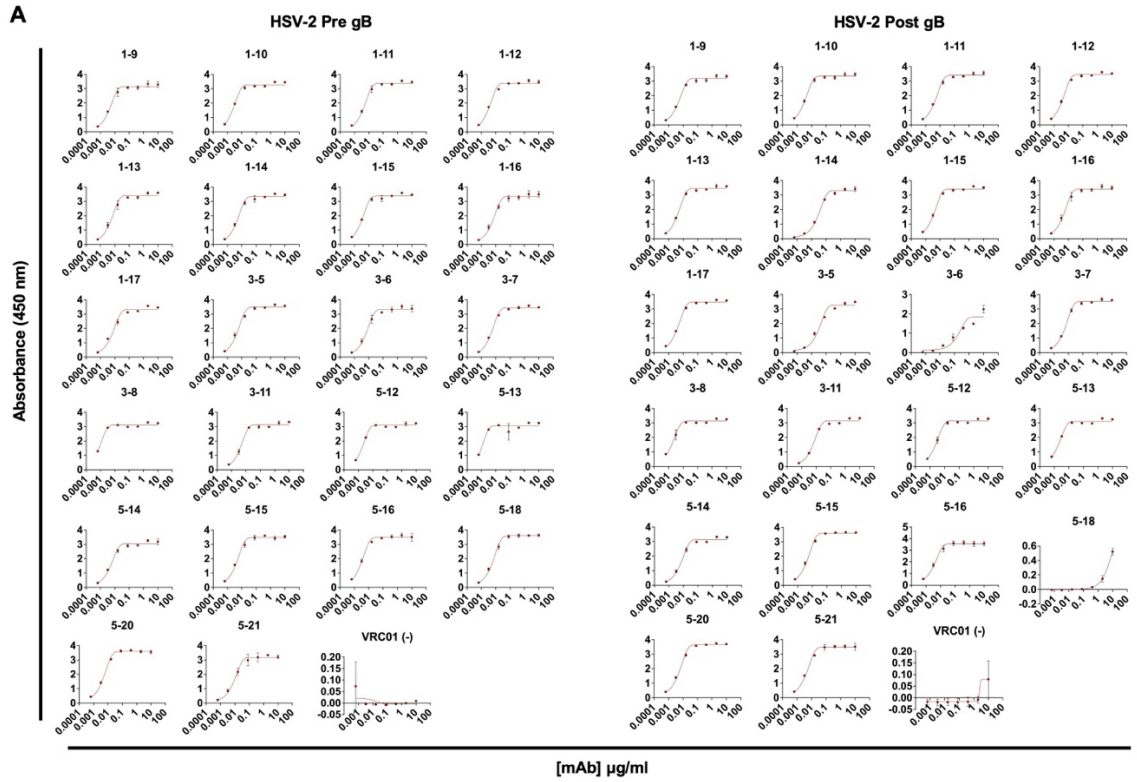

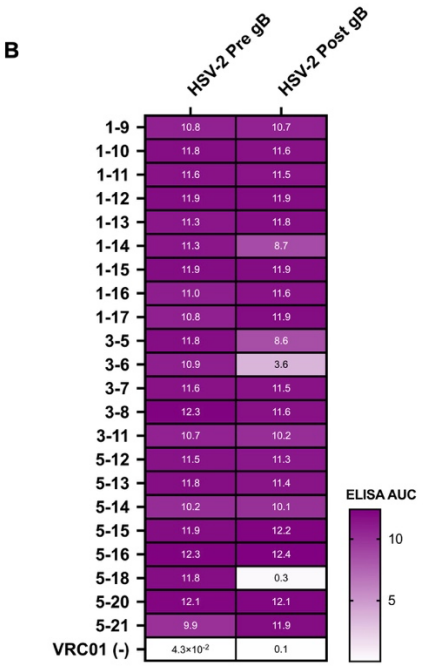

Fig. S2. Antibodies discovered by LIBRA-seq bind to HSV-2 pre- and postfusion gB. (A) Indirect ELISA absorbance measurement of recombinantly produced antibodies binding to HSV-2 prefusion or postfusion gB. **(B)** Area under the curve (AUC) of transformed absorbance values. Experiments were performed in technical and biological duplicates.

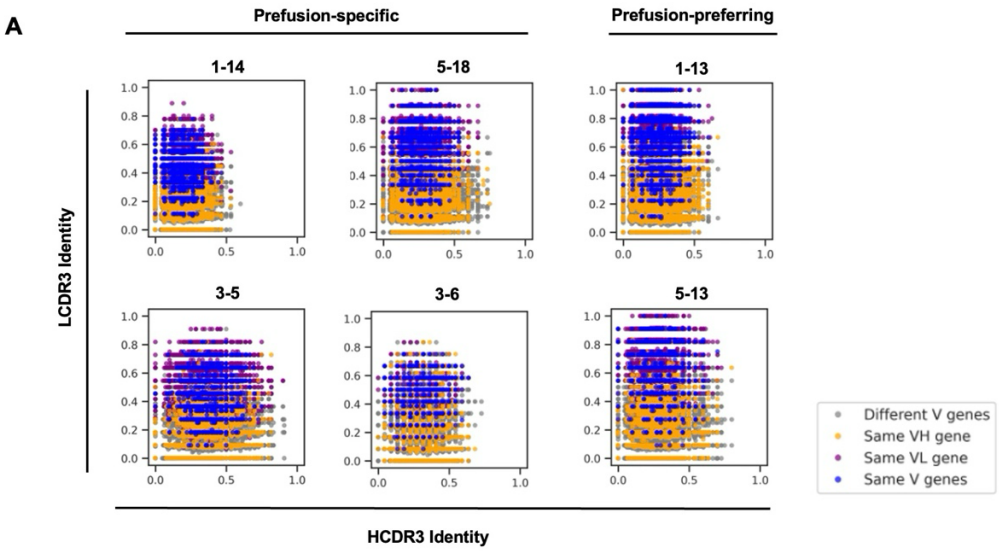

B

Summary counts of prefusion gB mAbs compared to database mAbs

mAb	HCDR3 ≥ 0.7	LCDR3 ≥ 0.7	HCDR3 + LCDR3 ≥ 0.7	Same VH gene	Same VL gene	Same VH + VL gene	VH Clones	Full Clones
1-13	0	45100	0	161443	81710	12390	0	0
1-14	0	388	0	129725	90365	9321	0	0
5-13	163	21090	4	81085	34635	2159	16	1
3-5	4498	4673	22	59763	95923	3258	203	0
3-6	2	538	0	134960	51924	4086	0	0
5-18	20	12307	0	85880	88942	5158	5	0

Fig. S3. Comparison of prefusion gB mAbs to published antibodies. (A) Sequence similarity of prefusion gB mAbs to a public database of 1.7 million paired antibody sequences. Each point represents an antibody from the database, compared with the prefusion gB mAb (represented by the title for each panel). Characterized by their identities in the CDR3 of the heavy chain (represented on the x-axis) and the light chain on the y-axis. The color coding of each dot in the plots corresponds to the matching of V genes between pairs of antibodies: Blue dots indicate identical use of both VH and VL genes; orange signifies matching VH gene use; purple represents matching VL gene use; and gray denotes cases in which neither VH nor VL genes match. **(B)** Shown are the counts based on comparisons shown in panel **A**. Full clones are defined as having matching V-gene usage and ≥ 0.7 CDR3 identity.

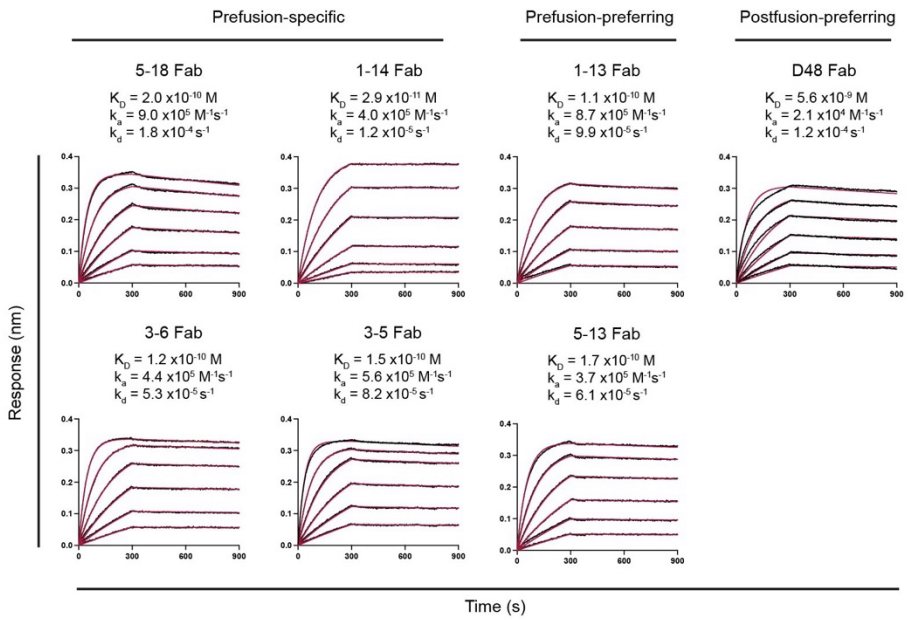

Fig. S4. Kinetics of isolated Fabs binding to HSV-2 prefusion stabilized gB. BLI sensorgrams for the association and dissociation kinetics of prefusion-specific and prefusion-preferring Fabs, as well as the postfusion-preferring control Fab D48, binding to HSV-2 prefusion-stabilized gB. Experimental data (black) were globally fit to a 1:1 binding model, with the fitted curves shown in red. The calculated values for K_d, k_a, and k_d are listed above each curve.

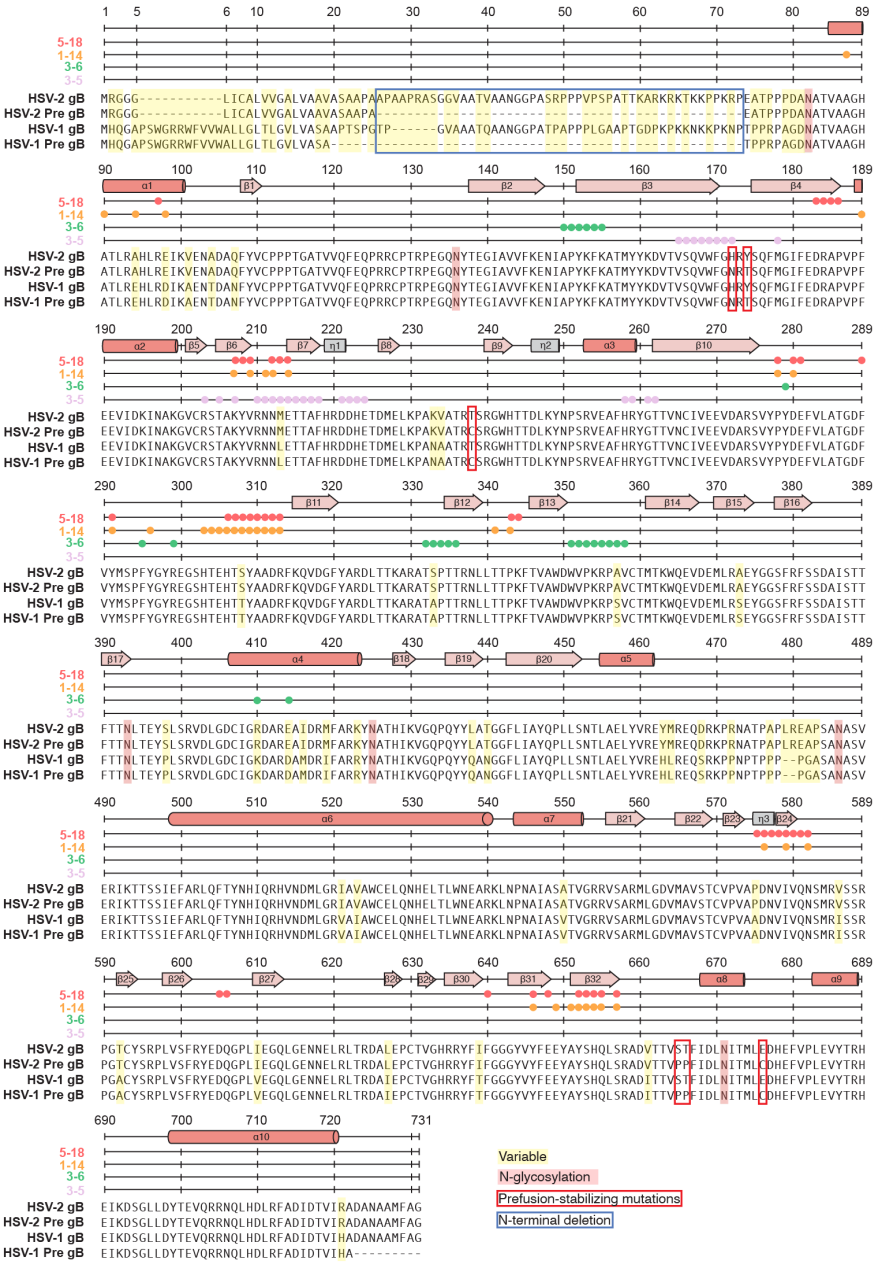

Fig. S5. Sequence alignment of HSV-2 and HSV-1 gB. Sequence alignment of HSV-2 gB ectodomain residues 1–731 and HSV-1 gB ectodomain residues 1–725. Residues involved in antibody interactions are indicated by colored circles above the alignment. Secondary structure elements were derived from the coordinates of HSV-2 gB bound to Fabs 3-5 and 3-6 and are annotated above the alignment. Variable positions between HSV-2 and HSV-1 gB are highlighted in yellow, *N*-linked glycosylation sites are in red, prefusion-stabilizing substitutions are annotated by red boxes, and the engineered N-terminal deletion is indicated by a blue box.

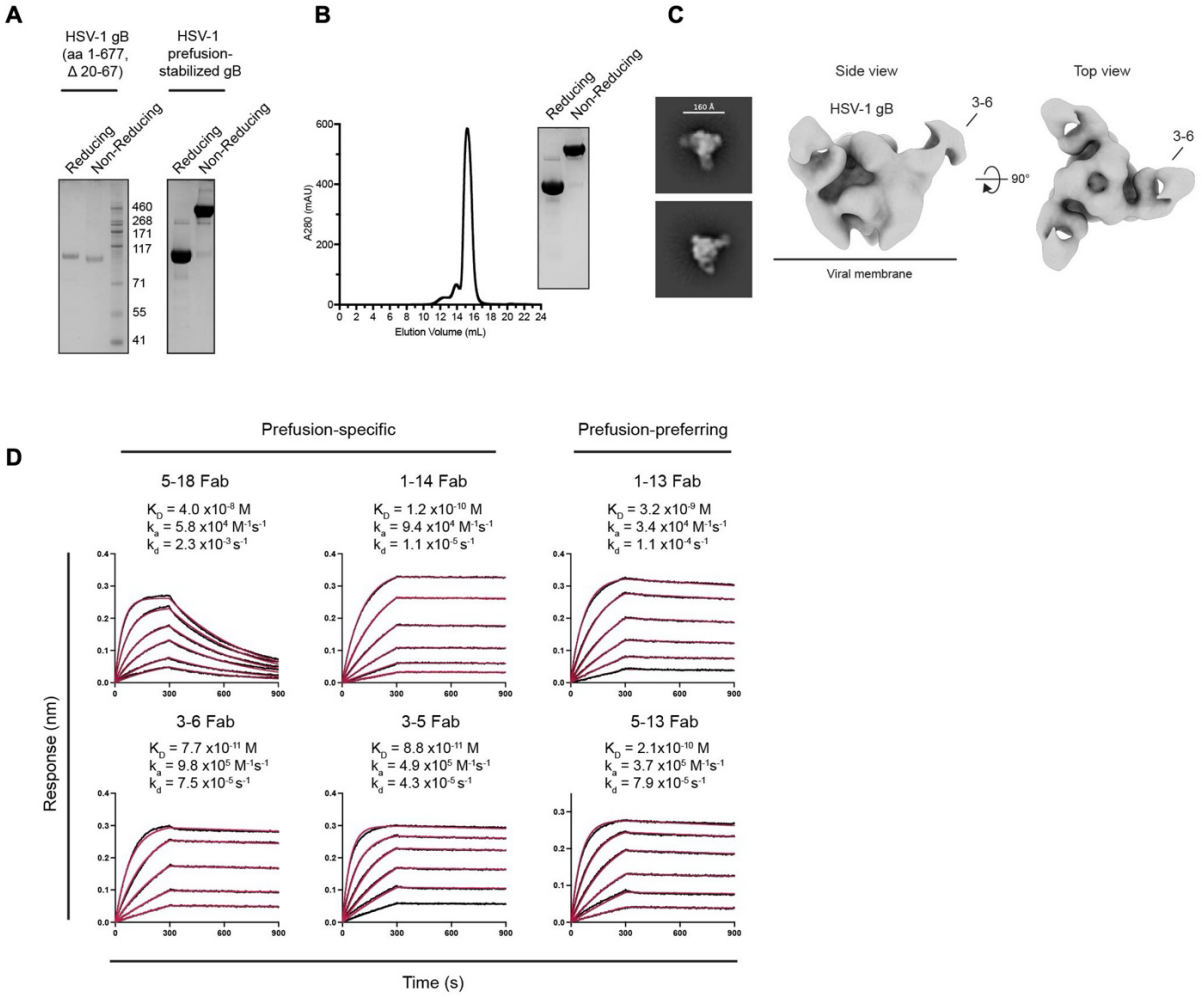

Fig. S6. Stabilization of HSV-1 prefusion gB and binding of prefusion-specific antibodies. (A) SDS-PAGE of HSV-1 gB constructs under reducing and non-reducing conditions. The stabilizing interprotomeric disulfide bond shifts the band to a molecular weight consistent with that of a trimer. **(B)** Size-exclusion chromatography (SEC) trace of prefusion-stabilized HSV-1 gB and SDS-PAGE of pooled SEC fractions under reducing and non-reducing conditions. **(C)** Negative-stain electron microscopy 2D-class averages and 3D-reconstruction volumes of HSV-1 prefusion-stabilized gB complexed with Fab 3-6. **(D)** BLI sensorgrams for the association and dissociation kinetics of prefusion-specific and prefusion-preferring Fabs binding to immobilized HSV-1 prefusion-stabilized gB on Ni^{2+}-NTA biosensors. Experimental data (black) were globally fit to a 1:1 binding model, with the fitted curves shown in red. The calculated values for the K_d, k_a, and k_d are listed above each curve.

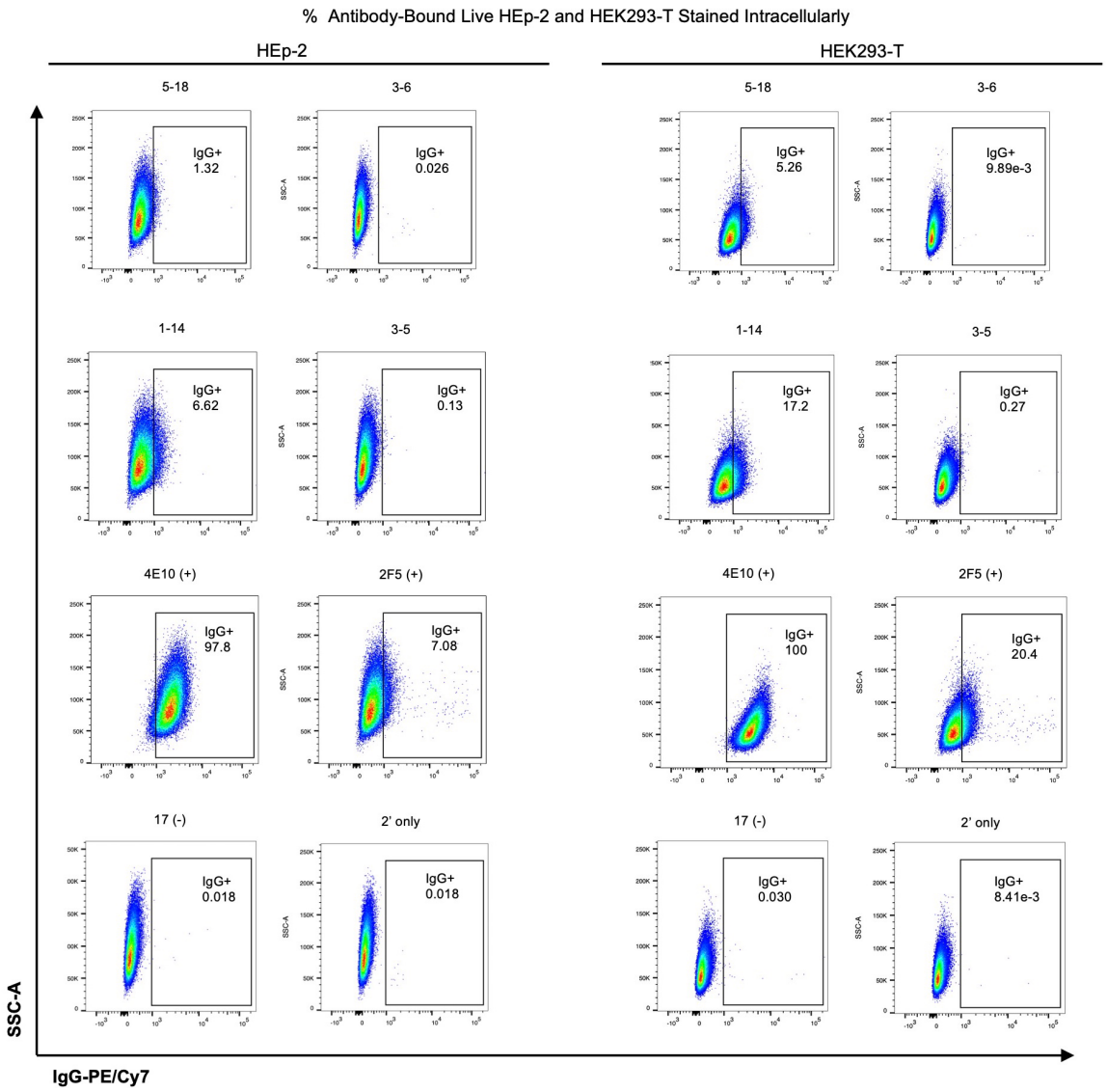

Fig. S7. Flow cytometry plots of intracellular self-antigen recognition by prefusion-specific mAbs. Representative flow cytometry plots for intracellular staining of HEp-2 cells and HEK293-T cells with 25 µg/mL positive control mAbs 4E10 and 2F5, negative control 17B, or experimental mAbs 5-18, 3-6, 1-14, and 3-5. Anti-human IgG Fc-PE/Cy7 was used to detect experimental and control recognition of cellular autoantigens.

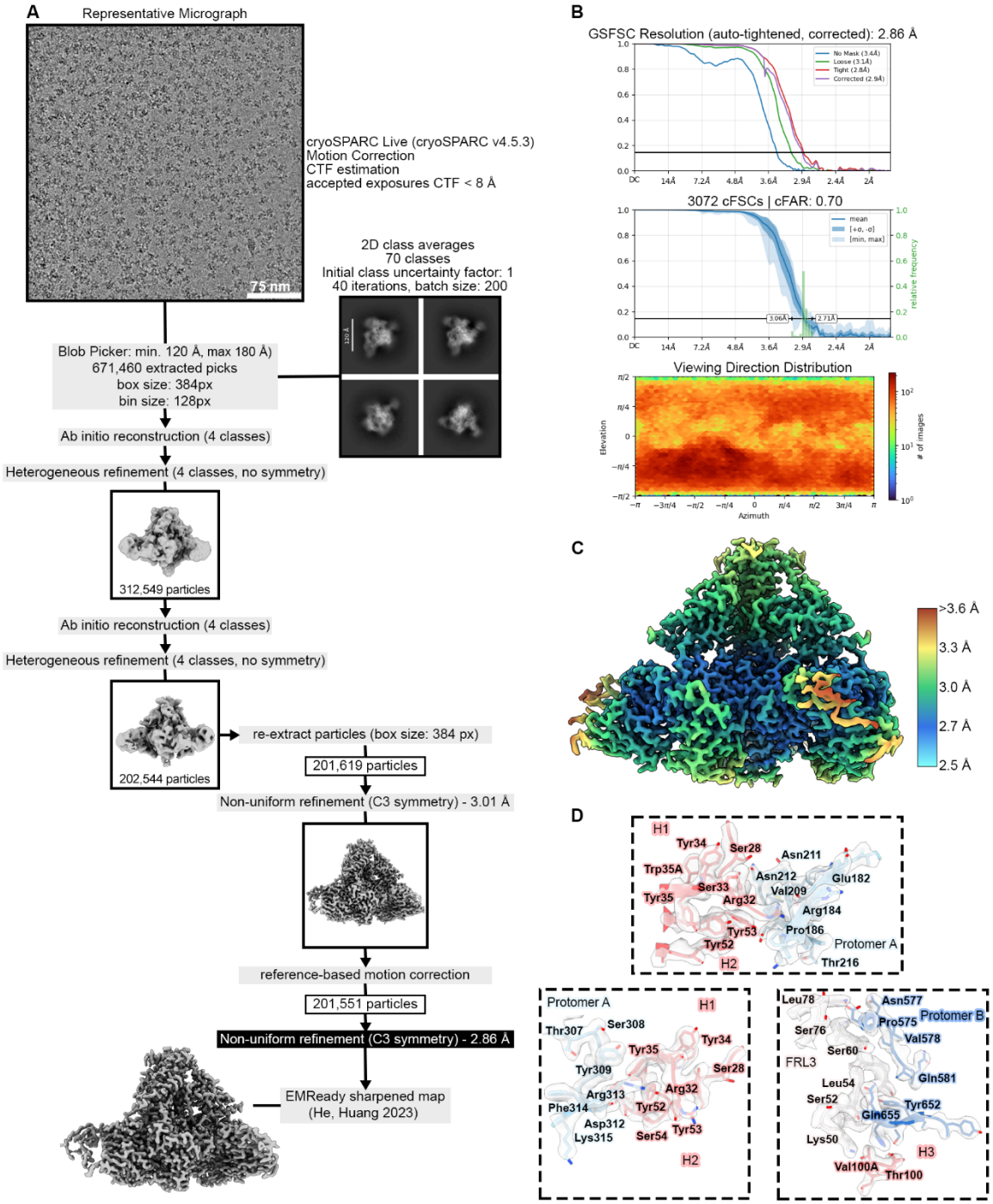

Fig. S8. Cryo-EM data processing workflow and structure validation for prefusion HSV-2 gB bound to Fab 5-18.

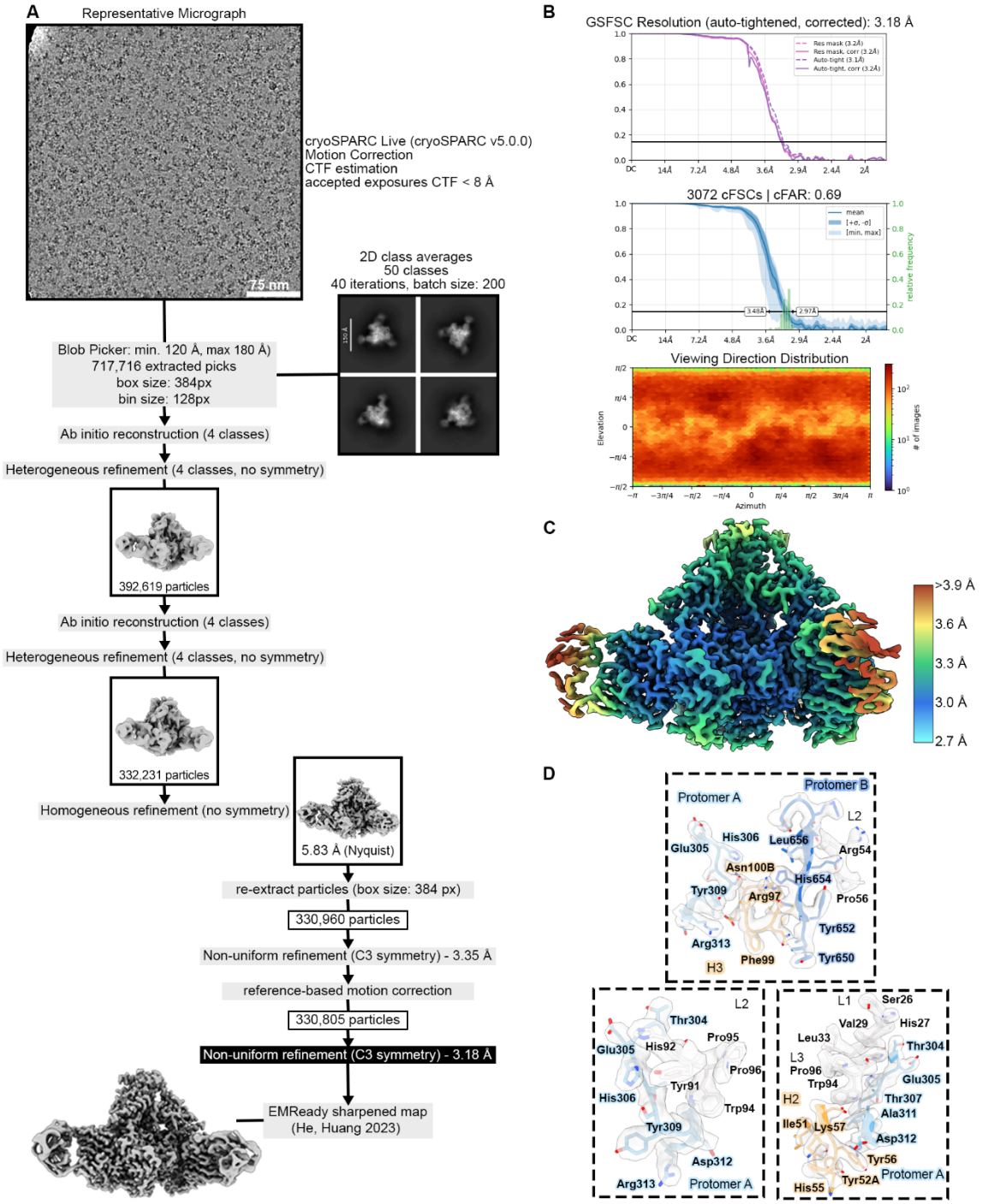

Fig. S9. Cryo-EM data processing workflow and structure validation for prefusion HSV-2 gB bound to Fab 1-14.

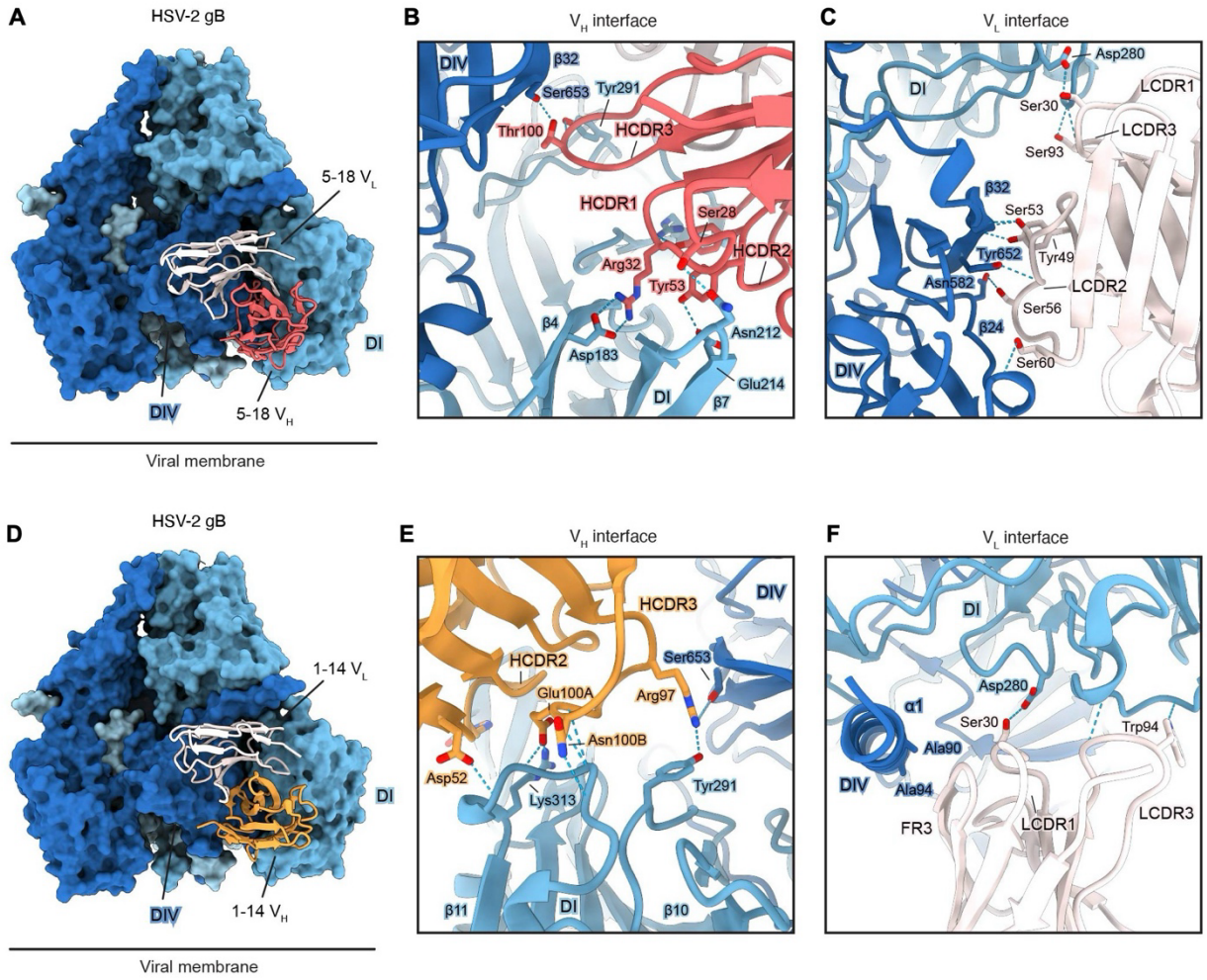

Fig. S10. Quaternary interfaces of prefusion-specific Fabs 5-18 and 1-14. (A), Side view of prefusion HSV-2 gB with one bound Fab 5-18. A horizontal black line indicates the approximate position of the viral membrane. **(B)** Magnified view of the 5-18 VH interface spanning Domain (D) I and DIV, depicted as ribbons. HCDR1 and HCDR2 contact DI through multiple hydrogen bonds and salt bridges, with $Arg32_{HCDR1}$ extending to engage the Asp183 sidechain in β4. HCDR3 spans DI and DIV, with $Thr100_{HCDR3}$ forming hydrogen bonds to Tyr291 in DI and Ser653 in DIV. **(C)** Magnified view of the 5-18 VL interface spanning DI and DIV, depicted as ribbons. LCDR1 and LCDR3 interact with DI, whereas LCDR2 engages β24 and β32 in DIV, forming a continuous hydrogen bond network. **(D)** Side view of prefusion HSV-2 gB with one bound Fab 1-14. **(E)** Magnified view of the 1-14 VH interface spanning DI and IV, depicted as ribbons. HCDR2 and HCDR3 mediate most contacts with the β10–β11 loop in DI. HCDR3 crosslinks DI and DIV, with $Arg97_{HCDR3}$ forming a hydrogen bond with the sidechain of Tyr291 in DI and Ser653 in DIV. **(F)** Magnified view of the 1-14 VL interface spanning DI and DIV, depicted as ribbons. LCDR1 and LCDR3 contact DI, whereas LCDR2 and FR3 make limited interactions with DIV, including the N-terminal α1 helix.

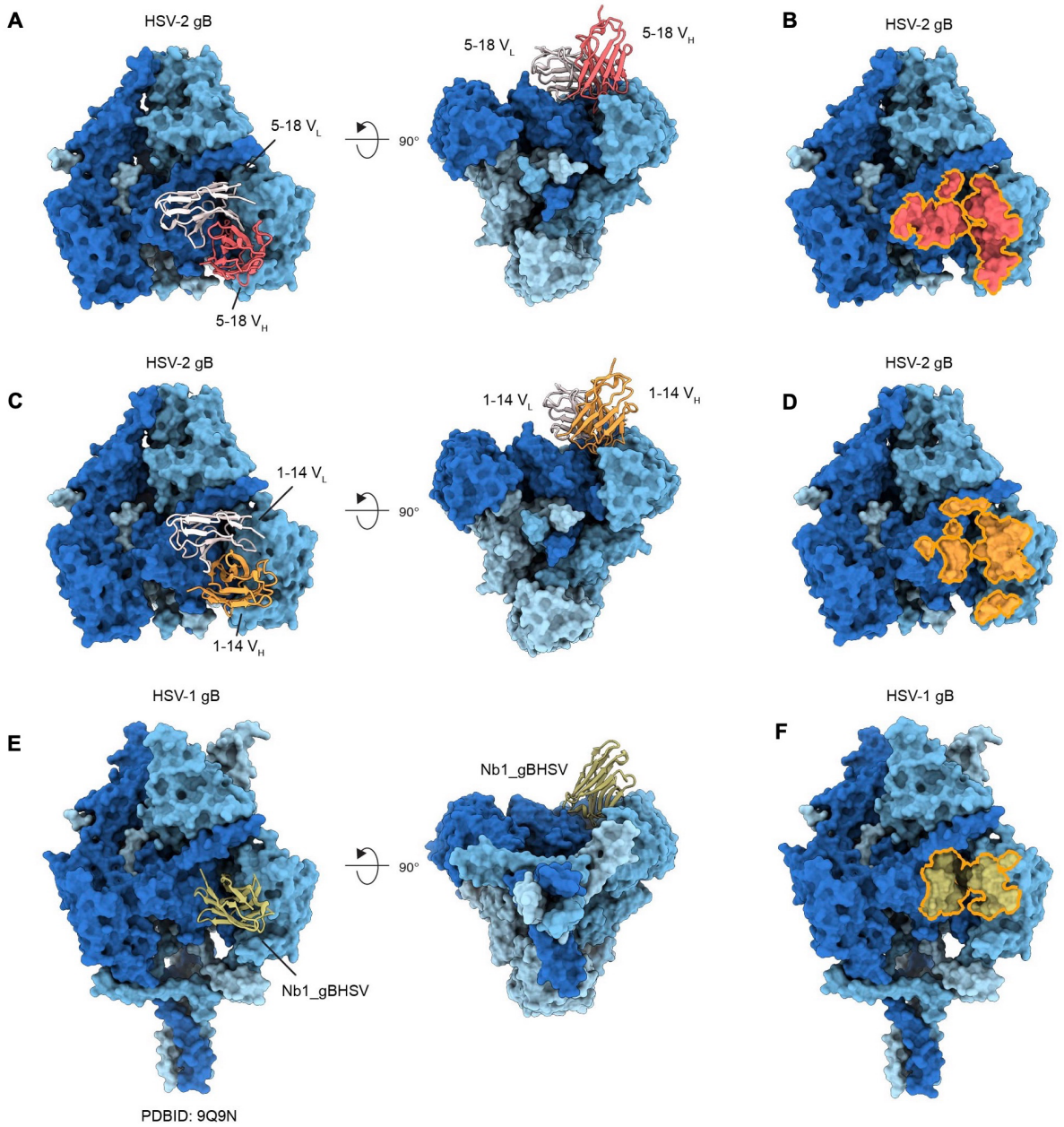

Fig. S11. Structural comparison of prefusion-specific Fabs 5-18, 1-14, and nanobody Nb1_gBHSV. **(A)** Side (*left*) and bottom (*right*) views of prefusion HSV-2 gB bound to Fab 5-18. **(B)** Side view showing the Fab 5-18 epitope footprint outlined in orange. **(C)** Side (*left*) and bottom (*right*) views of prefusion HSV-2 gB bound to Fab 1-14. **(D)** Side view showing the Fab 1-14 epitope footprint. **(E)** Side (*left*) and bottom (*right*) views of prefusion HSV-1 gB bound to nanobody Nb1_gBHSV (PDBID: 9Q9N). **(F)** Side view showing the Nb1_gBHSV epitope footprint**.**

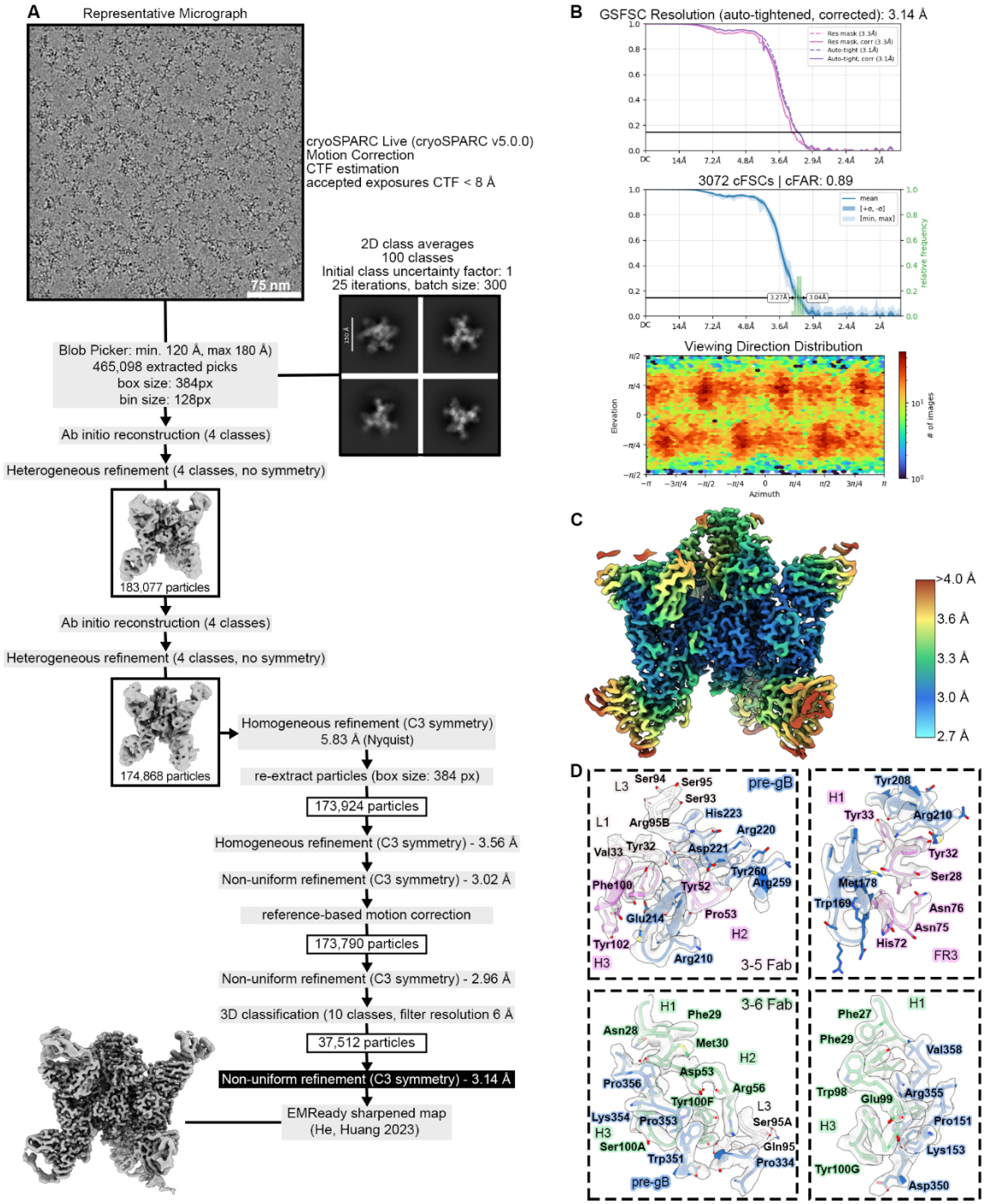

Fig. S12. Cryo-EM data processing workflow and structure validation for prefusion HSV-2 gB bound to Fabs 3-6 and 3-5.

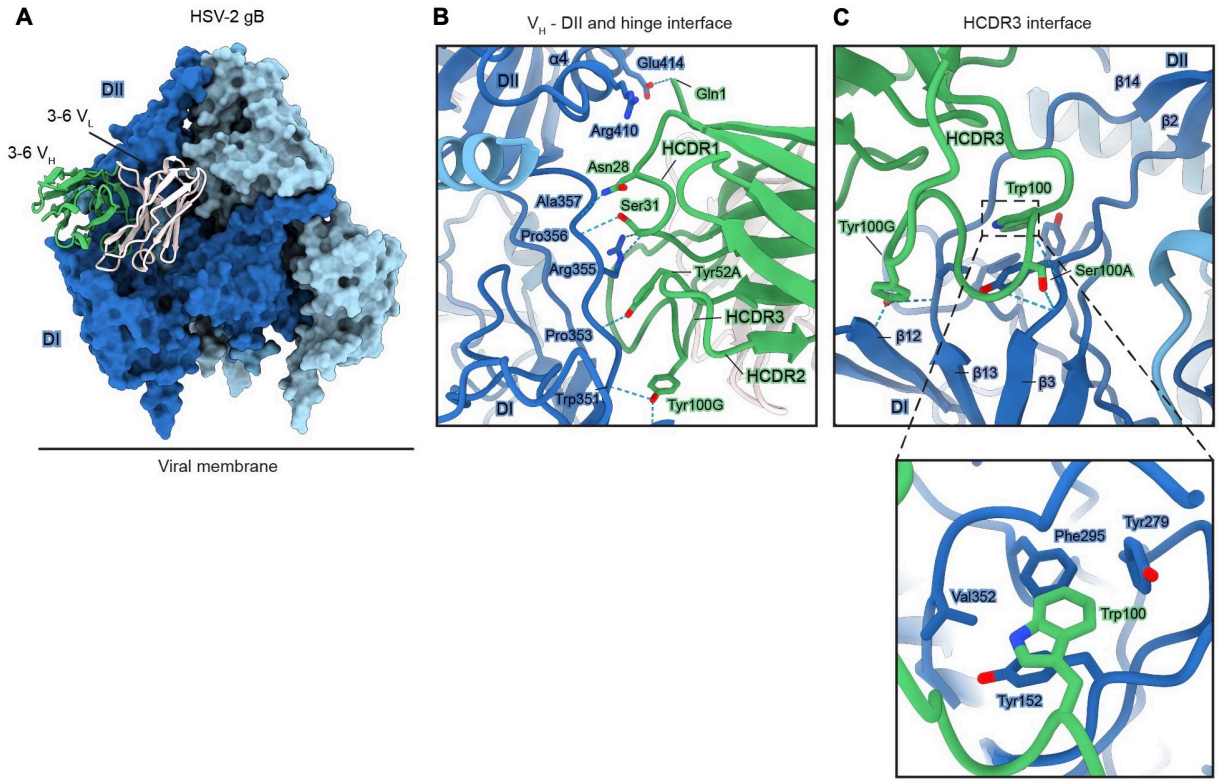

Fig. S13. Interface of prefusion-specific Fab 3-6 with prefusion HSV-2 gB. (A) Side view of prefusion HSV-2 gB with one bound Fab 3-6. The 3-6 VH is colored green, the 3-6 VL is colored white, and each protomer of prefusion gB is colored in a different shade of blue. A horizontal black line indicates the approximate position of the viral membrane. **(B)** Magnified view of the 3-6 VH interface with the domain (D)II and hinge region, depicted as ribbons. FR1 and HCDR1 of the heavy chain interact with the α4 helix of DII. HCDR1, HCDR2, and HCDR3 form hydrogen bonds with mainchain atoms in hinge residues 351–358 and the sidechain of Arg355. **(C)** Magnified view of HCDR3 interactions with DI, depicted as ribbons. HCDR3 contacts β2–β3 loop, β12, and the β13–β14 loop (hinge). The inset shows $Trp100_{HCDR3}$ inserted into a hydrophobic pocket formed by Tyr152, Tyr279, Phe295, and Val352.

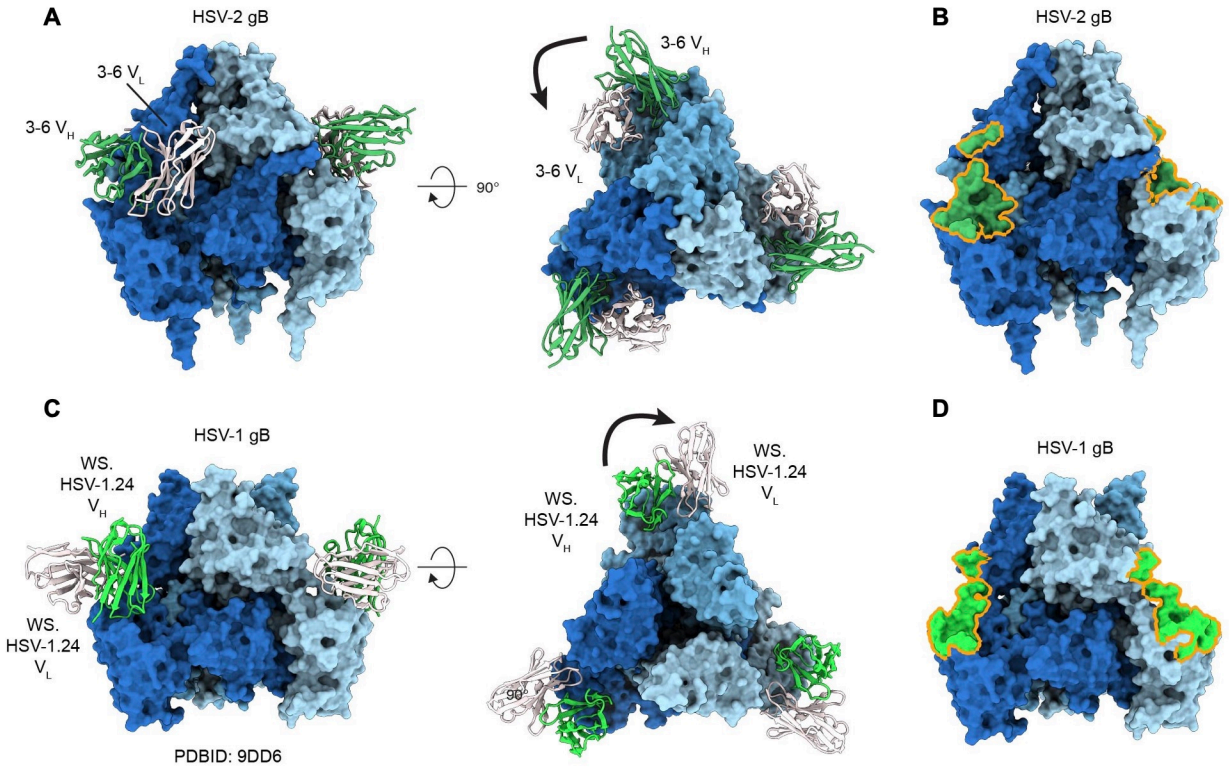

Fig. S14. Structural comparison of prefusion-specific Fab 3-6 and murine mAb WS.HSV-1.24. (A) Side (left) and bottom (right) views of prefusion HSV-2 gB with three bound Fab 3-6. The 3-6 VH is colored green, the VL is colored white, and gB protomers are colored shades of blue. **(B)** Side view showing the epitope footprint of Fab 3-6 on prefusion HSV-2 gB. Footprints are outlined in orange. **(C)** Side (left) and bottom (right) views of prefusion HSV-1 gB with three bound Fab WS.HSV-1.24 (PDB ID: 9DD6). The WS.HSV-1.24 VH is colored light green, the VL is colored white, and gB protomers are colored shades of blue. **(D)** Side view showing the epitope footprint of Fab WS.HSV-1.24 on prefusion HSV-1 gB.

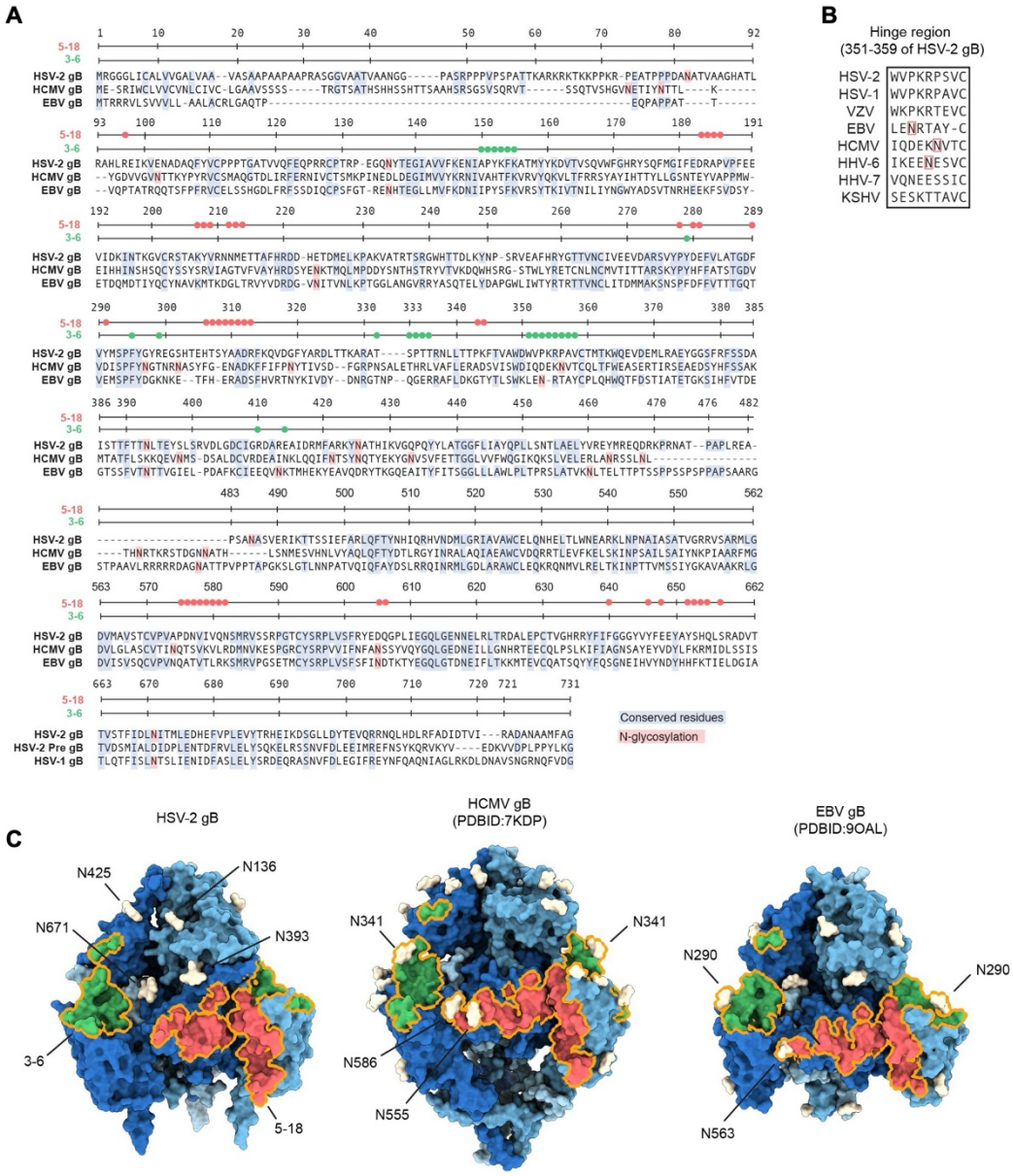

Fig. S15. Conservation and glycan shielding of HSV-2 prefusion-specific epitopes across human herpesvirus gBs . **(A)** Sequence alignment of HSV-2 gB residues 1–731 (strain HG52), HCMV gB residues 1–711 (strain Towne), and EBV gB residues 1–692 (strain M81). Residues in the prefusion-specific epitopes of mAbs 5-18 (red) and 3-6 (green) are indicated above the alignments by colored circles. Conserved residues among HSV-2, HCMV, and EBV gB are highlighted in blue, and *N*-linked glycosylation sites are shown in red. **(B)** Sequence alignment of the domain (D)I–DII hinge-region residues from human herpesvirus gBs, with *N*-linked glycosylation sites in the hinge regions indicated by red boxes. **(C)** Structural comparison of the glycan shield near prefusion-specific epitopes in HSV-2, HCMV, and EBV gB. HSV-2 gB glycans are modeled based on the HSV-2 gB–Fab 3-5 and 3-6 complex structure. HCMV gB (PDB ID: 7KDP) and EBV gB (PDB ID: 9OAL) *N*-linked glycans are modeled using the GlycoShape server. The Fab 5-18 footprint is shown in red, the Fab 3-6 footprint in green, and both footprints are outlined in orange. Glycans are colored white. All built glycans are labeled for HSV-2, while only shielding glycans are labeled for HCMV and EBV gB

Autoreactivity Summary Table – Intracellular and Extracellular IgG Binding (%)

mAb	HEp-2		HEK293-T	
	Intracellular (%)	Extracellular (%)	Intracellular (%)	Extracellular (%)
3-5	0.1	0.0	0.3	0.0
3-6	0.0	0.0	0.0	0.0
1-14	**6.6**	0.0	**17.2**	0.0
5-18	1.3	0.1	**5.3**	0.1
4E10 (+)	**97.8**	0.0	**100.0**	0.0
2F5 (+)	**7.1**	0.4	**20.4**	0.4
17B (-)	0.0	0.0	0.0	0.0
VRC01 (-)	**22.1**	0.0	**32.9**	0.0
2' only	0.0	0.0	0.0	0.0

Table S1. Summary table of flow cytometry assay for intracellular and extracellular self-antigen recognition by prefusion-specific mAbs. Shown is the percent of antibody-bound HEp-2 and HEK293T live cell lines stained with mAbs intracellularly and extracellularly and gated for IgG-positive cells. Positive cutoff for autoreactivity set at 5% (bold).

Fab 5-18

HSV-2 gB : Fab 5-18 V_H

Protomer A

Hydrogen bonds

	Protomer A	Atom	Dist. [Å]	5-18 V_H	Atom	Position
1	ASN 212	[OD1]	3.11	SER 28	[OG]	HCDR1
2	ASP 183	[OD1]	3.14	ARG 32	[NH1]	HCDR1
3	ASP 183	[OD2]	2.96	ARG 32	[NH2]	HCDR1
4	ARG 184	[O]	3.85	ARG 32	[NH1]	HCDR1
5	LYS 207	[O]	3.52	ARG 32	[NH2]	HCDR1
5	ARG 313	[NH2]	3.85	ARG 32	[O]	HCDR1
6	ARG 313	[NH1]	2.87	TYR 35	[OH]	HCDR1
7	ARG 313	[NH2]	3.18	TYR 52	[OH]	HCDR2
8	GLU 214	[OE2]	3.35	TYR 53	[OH]	HCDR2
9	ASP 312	[OD2]	2.70	TYR 58	[OH]	HCDR2
11	TYR 291	[OH]	2.85	THR 100	[O]	HCDR3

Salt bridges

	Protomer A	Atom	Dist. [Å]	5-18 V_H	Atom	Position
1	ASP 183	[OD1]	3.88	ARG 32	[NH2]	HCDR1
2	ASP 183	[OD1]	3.14	ARG 32	[NH1]	HCDR1
3	ASP 183	[OD2]	2.96	ARG 32	[NH2]	HCDR1
4	ASP 183	[OD2]	3.57	ARG 32	[NH1]	HCDR1

Protomer C

Hydrogen bonds

	Protomer C	Atom	Dist. [Å]	5-18 V_H	Atom	Position
1	SER 653	[OH]	2.62	THR 100	[OG1]	HCDR3

HSV-2 gB : Fab 5-18 V_L

Protomer A

Hydrogen bonds

	Protomer A	Atom	Dist. [Å]	5-18 V_L	Atom	Position
1	ASP 280	[OD2]	2.8	SER 30	[OG]	LCDR1
2	SER 308	[O]	3.1	SER 93	[N]	LCDR3
3	SER 308	[O]	2.82	SER 93	[OG]	LCDR3

Protomer C

Hydrogen bonds

	Protomer C	Atom	Dist. [Å]	5-18 V_L	Atom	Position
1	SER 653	[O]	2.63	TYR 49	[OH]	LCDR2
2	GLN 655	[N]	2.99	SER 53	[OG]	LCDR2
3	GLN 655	[O]	3.38	SER 53	[OG]	LCDR2
4	TYR 652	[OH]	2.74	LEU 54	[O]	LCDR2
5	TYR 652	[OE1]	3.72	LEU 54	[N]	LCDR2
6	ASN 582	[OD1]	3.34	SER 56	[OG]	LCDR2
7	VAL 580	[O]	3.83	GLY 57	[N]	LCDR2
8	ASP576	[O]	3.72	SER 60	[OG]	LCDR2
9	ASP 576	[O]	3.41	ARG 61	[N]	LCDR2

Fab 1-14

HSV-2 gB : Fab 1-14 V_H

Protomer A

Hydrogen bonds

	Protomer A	Atom	Dist. [Å]	1-14 V_H	Atom	Position
1	PRO 343	[O]	3.9	TYR 52A	[OH]	HCDR2
2	GLU 214	[OE1]	3.27	HIS 55	[NE2]	HCDR2
3	ALA 311	[N]	3.03	ASP 58	[OD2]	HCDR2
4	ASN 212	[ND2]	2.85	SER 74	[OG]	H-FR3
5	TYR 291	[OH]	2.84	ARG 97	[NH2]	HCDR3
6	SER 308	[O]	3.12	GLU 100A	[N]	HCDR3
7	ALA 310	[N]	2.88	GLU 100A	[OE2]	HCDR3
8	ARG 313	[NH1]	3.15	GLU 100A	[OE1]	HCDR3
9	ARG 313	[NH1]	3.13	GLU 100A	[OE2]	HCDR3
10	THR 307	[O]	2.99	ASN 100B	[ND2]	HCDR3
11	SER 308	[O]	2.98	ASN 100B	[ND2]	HCDR3

Salt bridges

	Protomer A	Atom	Dist. [Å]	1-14 V_H	Atom	Position
1	GLU 214	[OE1]	3.27	HIS 55	[NE2]	HCDR2
2	ARG 313	[NH1]	3.15	GLU 100A	[OE1]	HCDR3
3	ARG 313	[NH1]	3.13	GLU 100A	[OE2]	HCDR3

Protomer C

Hydrogen bonds

	Protomer C	Atom	Dist. [Å]	1-14 V_H	Atom	Position
1	SER 653	[OG]	3.8	ARG 97	[NH2]	HCDR3
2	TYR 652	[O]	3.76	GLN 98	[NE2]	HCDR3

HSV-2 gB : Fab 1-14 V_L

Protomer A

Hydrogen bonds

	Protomer A	Atom	Dist. [Å]	1-14 V_L	Atom	Position
1	ASP 280	[OD2]	2.89	SER 30	[OG]	LCDR1
2	THR 307	[N]	3.08	HIS 92	[O]	LCDR3
3	TYR 309	[O]	2.85	TRP 94	[NE1]	LCDR3

Table S2. Interface analysis of mAbs 5-18 and 1-14 with prefusion stabilized HSV-2 gB. (PDBePISA)

Fab 3-6

HSV-2 gB : Fab 3-6 V_H

Hydrogen bonds

	Protomer A	Atom	Dist. [Å]	3-6 V_H	Atom	Position
1	GLU 414	[OE1]	3.53	GLN 1	[N]	H-FR1
2	ALA 357	[O]	2.98	ASN 28	[ND2]	H-FR1
3	VAL 358	[O]	3.84	ASN 28	[ND2]	H-FR1
4	ARG 355	[NE]	2.86	SER 31	[O]	HCDR1
5	ARG 355	[NH2]	2.87	SER 31	[O]	HCDR1
6	PRO 356	[O]	2.71	SER 31	[OG]	HCDR1
7	PRO 353	[O]	2.84	TYR 52A	[OH]	HCDR2
8	PRO 334	[O]	2.97	ARG 56	[NH1]	HCDR2
9	LYS 153	[N]	3.46	TRP 100	[O]	HCDR3
10	LYS 153	[O]	2.82	SER 100A	[OG]	HCDR3
11	LYS 153	[O]	2.85	GLY 100B	[N]	HCDR3
12	TYR 336	[N]	3.21	GLY 100C	[N]	HCDR3
13	THR 336	[N]	3.21	TYR 100 G	[OH]	HCDR3
14	TRP 351	[O]	2.92	TYR 100 G	[OH]	HCDR3
15	ARG 299	[NH1]	3.75	TYR 100 F	[OH]	HCDR3

Salt bridges

	Protomer A	Atom	Dist. [Å]	3-6 V_H	Atom	Position
1	GLU 414	[OE1]	3.53	GLN 1	[N]	H-FR1

HSV-2 gB : Fab 3-6 V_L

Hydrogen bonds

	Protomer A	Atom	Dist. [Å]	3-6 V_H	Atom	Position
1	SER 333	[OG]	3.65	ASP 93	[O]	LCDR3

Fab 3-5

HSV-2 gB : Fab 3-5 V_H

Hydrogen bonds

	Protomer A	Atom	Dist. [Å]	3-5 V_H	Atom	Position
1	VAL 168	[O]	3.86	SER 30	[O]	HCDR1
2	MET 178	[SD]	3.75	SER 30	[OG]	HCDR1
3	ARG 210	[O]	2.8	TYR 32	[OH]	HCDR1
4	ASN 211	[O]	3.81	TYR 32	[OH]	HCDR1
5	THR 216	[O]	3.79	TYR 33	[OH]	HCDR1
6	VAL 168	[N]	3.63	PRO 53	[O]	HCDR2
7	PHE 170	[N]	3.01	THR 73	[OG1]	H-FR3
8	PHE 170	[O]	3.16	THR 73	[N]	H-FR3
9	PHE 170	[O]	2.86	THR 73	[OG1]	H-FR3
10	PHE 170	[O]	3.7	SER 74	[N]	H-FR3
11	GLU 214	[O]	3.25	ARG 94	[NH1]	HCDR3
12	GLU 214	[O]	2.91	ARG 94	[NH2]	HCDR3
13	THR 215	[OG1]	2.87	ARG 94	[NH2]	HCDR3
14	THR 216	[N]	2.99	SER 96	[O]	HCDR3
15	GLU 214	[O]	3.66	TYR 99	[OH]	HCDR3
16	GLU 214	[OE2]	3.19	TYR 102	[OH]	HCDR3

HSV-2 gB : Fab 3-5 V_L

Hydrogen bonds

	Protomer A	Atom	Dist. [Å]	3-5 V_L	Atom	Position
1	GLU 224	[O]	2.82	TYR 30	[OH]	LCDR1
2	ARG 203	[NH2]	3.24	ASN 31	[OD1]	LCDR1
3	THR 205	[OG1]	2.96	TYR 32	[OH]	LCDR1
4	GLU 224	[OE2]	2.74	TYR 32	[OH]	LCDR1
5	ASP 221	[O]	3.12	ARG 95B	[NH1]	LCDR3
6	ASP 221	[O]	2.82	ARG 95B	[NH2]	LCDR3
7	ASP 222	[OD1]	3.78	ARG 95B	[NH2]	LCDR3

Salt bridges

	Protomer A	Atom	Dist. [Å]	3-5 V_L	Atom	Position
1	ASP 222	[OD1]	3.78	ARG 95B	[NH2]	LCDR3

Table S3. Interface analysis of mAbs 3-5 and 3-6 with prefusion-stabilized HSV-2 gB (PDBePISA).

Sample	gB-G3 (prefusion HSV-2 gB) + 5-18 Fab	gB-G3 (prefusion HSV-2 gB) + 1-14 Fab	gB-G3 (prefusion HSV-2 gB) + 3-6 and 3-5 Fabs
PDB ID	10UD	11AB	11BH
EMDB code	EMD-75469	EMD-75581	EMD-75602
Cryo-EM data collection			
Microscope	FEI Glacios	FEI Glacios	FEI Glacios
Voltage (kV)	200	200	200
Detector	Falcon 4	Falcon 4	Falcon 4
Magnification (nominal)	150,000	150,000	150,000
Pixel size (Å/pix)	0.933	0.933	0.933
Exposure dose ($e^-/Å^2$)	49	49	49
Defocus range (μm)	1.5 – 2.5	1.5 – 2.5	0.0 – 1.0
Tilt angle (°)	30	30	0
Micrographs collected	2,551	2,553	3,060
Micrographs used	1,780	2,413	2,244
Particles extracted	672,460	717,716	465,098
Automation software	SerialEM	SerialEM	SerialEM
3D reconstruction statistics			
Particles	201,551	330,805	37,512
Symmetry	C3	C3	C3
Map sharpening B-factor	128.1	160.3	91.0
Unmasked: 0.5	3.8	3.8	4.3
Masked: 0.5	3.2	3.5	3.6
Unmasked: 0.143	3.4	3.6	3.7
Masked: 0.143	2.9	3.2	3.1
Model refinement and validation statistics			
Sharpening tool	EMReady v2.2.2	EMReady v2.2.2	EMReady v2.2.2
Refinement package	PHENIX	PHENIX	PHENIX
Composition			
Non-hydrogen atoms	19,824	19,656	25,491
Amino Acids	2,487	2,466	3,225
Ligands (type)	6 (6 NAG)	3 (3 NAG)	15 (3 BMA, 12 NAG)
Bonds (RMSD)			
Length (Å)	0.005	0.004	0.004
Angles (°)	0.97	0.947	0.948
Ramachandran plot			
Favored (%)	97.52	97.45	97.65
Allowed (%)	2.48	2.55	2.35
Outliers (%)	0.0	0.0	0.0
Rotamer outliers (%)	0.0	0.09	0.11
Cβ outliers (%)	0.0	0.0	0.0
CaBLAM outliers (%)	1.03	2.34	1.36
ADP (B-factors)			
Amino Acids (mean)	42.1	75.0	69.8
Ligands (mean)	101.6	97.1	130.3
CC (mask)	0.89	0.89	0.89
MolProbity score	1.15	1.20	1.06
Clash score	2.61	3.03	2.08
Overall mean Q-Score	0.67	0.60	0.58

Table S4. Cryo-EM Data collection and refinement statistics.